$BVRI$ Surface Photometry of Isolated Spiral Galaxies[1]

H. M. Hernández-Toledo[1] J. Zendejas-Domínguez[2] and V. Avila-Reese[3]

Instituto de Astronomía, Universidad Nacional Autónoma de México, A.P. 70-264, 04510 México D. F., México

ABSTRACT

A release of multicolor broad band ($BVRI$) photometry for a subsample of 44 isolated spirals drawn from the *Catalogue of Isolated Galaxies* (CIG) is presented. Total magnitudes and colors at various circular apertures, as well as some global structural/morphological parameters are estimated. Morphology is reevaluated through optical and sharp/filtered R band images, $(B-I)$ color index maps, and archive near–IR JHK images from the Two–Micron Survey. The CAS structural parameters (Concentration, Asymmetry, and Clumpiness) were calculated from the images in each one of the bands. The fraction of galaxies with well identified optical/near–IR bars (SB) is 63%, while a 17% more shows evidence of weak or suspected bars (SAB). The sample average value of the maximum bar ellipticity is $\epsilon_{\rm max} \approx 0.4$. Half of the galaxies in the sample shows rings. We identify two candidates for isolated galaxies with disturbed morphology. The structural CAS parameters change with the observed band, and the tendencies they follow with the morphological type and global color are more evident in the redder bands. In any band, the major difference between our isolated spirals and a sample of interacting spirals is revealed in the $A-S$ plane. A deep and uniformly observed sample of isolated galaxies is intended for various purposes including (i) comparative studies of environmental effects, (ii) confronting model predictions of galaxy evolution and (iii) evaluating the change of galaxy properties with redshift.

Subject headings: Galaxies: spiral – Galaxies: irregulars – Galaxies: structure – Galaxies: photometry – Galaxies: interactions – Galaxies: morphology

1. Introduction

The concept of a "field" population of galaxies as distinct from the group/cluster populations has existed since the earliest days of extragalactic astronomy (Hubble 1936) and it is used recurrently in studies aimed to explore the effects of large–scale environment on galaxy properties. However, the definition of "field" is fuzzy. The distribution of galaxies in space is actually strongly clustered

[1]E-mail: hector@astroscu.unam.mx

[2]E-mail: zendejas@astroscu.unam.mx

[3]E-mail: avila@astroscu.unam.mx

[1]Based on data obtained at the 0.84m and 1.5m telescopes of the Observatorio Astronómico Nacional, San Pedro Mártir, Baja California, México, operated by the Instituto de Astronomía, Universidad Nacional Autónoma de México.

and a large fraction of them is prone to form gravitationally-bound multiple systems, from very populated clusters to loose groups, the majority being in normal groups (Tully 1987). *Isolation* is an important requirement beyond the concept of "field" galaxies. A galaxy is isolated if it has not suffered any interaction with another normal galaxy or with a group environment over a Hubble time or at least since approximately one half of its mass was assembled. This makes the observational finding and study of isolated galaxies important because, among other reasons, (i) they can be used as comparison objects in studies of the environmental effects on galaxies belonging to groups and clusters, and (ii) they are ideal for confronting with theoretical and model predictions of galaxy evolution.

The fact that properties of galaxies change with environment has been known for a long time. The main observable dependencies with environment –from cluster centers to the sparse "field"– are seen for the morphological mix, the global colors, and the specific star formation (SF) rate; for recent reviews see Park et al. (2007), Avila-Reese et al. (2005), and the references therein. These properties are inferred mainly from photometric observations. In fact, to study observationally the effects of high–density environments on the galaxy properties, a good understanding of the isolated, non–perturbed, galaxies is necessary. These galaxies are also required as a control sample for studying interacting galaxies. For example, in Hernández-Toledo et al. (2005; see also Conselice 2003) we have compared the photometric concentration, asymmetry and clumpiness parameters of local interacting and "field" disk galaxies with the aim to establish a relatively easy way for identifying interacting disk galaxies in high–redshfit samples.

Among isolated galaxies, the observational study of disk galaxies is of special interest because, on one hand, they are expected to be more drastically affected by environmental and interaction effects; on the other hand, according to the current paradigm of cosmic structure formation, the formation of disks inside hierarchically growing Cold Dark Matter (CDM) haloes is a generic process. A large amount of work has been done in modeling the evolution of (isolated) disk galaxies. Well observed samples of isolated disk galaxies are hence important in order to confront with model predictions (e.g., Avila–Reese & Firmani 2000; Cole et al. 2000; Boissier & Prantzos 2000; Firmani & Avila–Reese 2000; Yang, Mo & van den Bosch 2003; Zavala et al. 2003; Pizagno et al. 2005; Dutton et al. 2006; Kassin, de Jong & Weiner 2006; Gnedin et al. 2006).

A uniformly selected and observed sample of isolated disk galaxies is also crucial for studying intrinsic secular processes able to affect the structure, morphology and dynamics of galaxies, for instance, the formation and evolution of bars, circular rings, lopsidedness, and bulges. However, chances are that isolated galaxies may show evidence of disturbances not associated with intrinsic processes, which opens the necessity to explore other alternatives. On this line, cosmological numerical simulations within the CDM model show that inside the galaxy–size haloes there survives a large population of subhaloes (Klypin et al. 1999; Moore et al. 1999), but reionization and feedback could inhibit the formation of luminous (satellite) galaxies inside most of these subhaloes (e.g., Bullock, Kravtsov & Weinberg 2000; Benson et al. 2002). The subhalos and the associated gas clouds could produce signs of distortion on isolated galaxies (Threntam, Moller & Ramirez-Ruiz 2001; Pisano, Wilcots & Liu 2002). If these signs are clear, then observations in radio could reveal the presence of 21–cm hydrogen line emission associated to a pure gas companion galaxy.

But if such an emission is absent, there is still the possibility that the 'perturber' is just a dark matter (sub)halo without any baryonic component (Threntam et al. 2001). Recently, Karachentsev, Karachentseva & Huchtmeier (2006), by analyzing a large sample of isolated galaxies, have reported the finding of four such possible cases.

Homogeneous observational data samples of isolated disk galaxies are crucial for obtaining transparent scaling relationships and correlations that can be appropriately confronted with model predictions (see, e.g. Zavala et al. 2003). In recent years, some groups have been working on the compilation and observation of such samples (e.g., Pisano et al. 2002; Allam et al. 2005; Koopmann & Kenney 2006). For galaxies in voids, which are the most likely to be isolated, see Rojas et al. (2004,2005). It is worth to mention that the important requirements for all these samples are: well defined and strong isolation criteria, a uniform-quality data acquisition in several wavelengths, and completeness when possible.

We have carried out optical CCD photometry for a representative set of galaxies in the northern Catalogue of Isolated Galaxies (hereafter CIG, Karachentseva 1973). This is one of the best defined and most complete catalogues of isolated galaxies. The aim of this paper is to present a global $BVRI$ photometric and morphological analysis for a subsample of 44 spiral galaxies from the CIG catalog. It is strongly emphasized that all the observations were done with the same CCD detector. After applying uniform reduction and analysis procedures, an homogeneous set of photometric and morphological data is guaranteed. CIG galaxies cover a wide range in luminosities, surface brightnesses, morphological types and colors. Their relative simplicity and closeness, as compared with galaxies in other environments, offer a unique opportunity to have a more detailed and less confused interpretation of their structural, photometric and morphological properties.

The outline of the paper is as follows. Section 2 summarizes the selection criteria applied to the isolated galaxy sample that are relevant to our photometric study, and describes the observations and reduction techniques used here. Section 3 presents a comparison of our estimated total magnitudes against those in the literature. In Section 4, we discuss the observed morphology based on mosaic $R-$band and $R-$band Sharp/filtered images, $(B - I)$ color index maps, and composed near–infrared (NIR) JHK images extracted from the Two–Micron Survey archives. Emphasis is put on the presence of disturbed morphology. Section 5 presents our estimates of the optical $(BVRI)$ and NIR $JK-$band concentration, asymmetry, and clumpiness (CAS) structural parameters. In Section 6 we explore and discuss some basic correlations among the $BVRI - JK$ photometric and structural parameters in this sample that could be useful for comparative studies involving galaxies in other environments. Section 7 provides a summary of the paper. Finally, an Appendix is devoted to the presentation of $BVRI$ magnitudes at two other concentric circular apertures.

2. The Data Sample

2.1. Isolated Spiral Galaxies from Karachentseva Catalogue.

We have carried out an observational program at the Observatorio Astronómico Nacional at San Pedro Mártir (OAN-SPM), Baja California, México, devoted to obtain uniform CCD photometric data for one of the most complete and homogeneous samples of isolated galaxies currently available, the CIG catalogue of Karachentseva (1973). This sample amounts to more than 1050 galaxies in the northern hemisphere. The CCD $BVRI$ im-

ages in the Johnson-Cousins system were obtained with a Site1 detector attached to the 1.5m and 0.84m telescopes at OAN-SPM covering an area of about $4.3' \times 4.3'$ and $7.2' \times 7.2'$, a typical seeing of 1.7 arcsec and a scale of $0.51''$/pixel and $0.85''$/pixel respectively.

The original number of galaxies in three observing runs amounts to 52 galaxies. From these, 6 galaxies obtained under bad observing conditions and 2 ellipticals were eliminated, yielding a final sample of 44 isolated spiral galaxies of the present study. We applied no special strategy in selecting this current subset. Availability of observing time and weather conditions were the main factors constraining the number of observed galaxies. Some aspects of the selection criteria for the CIG sample that are most relevant to the present and further photometric analyses are stated here.

The isolated galaxies in the CIG sample were selected from a visual search of the Palomar Sky Survey. The catalogue samples the sky north of $\delta \geq -3°$. The vast majority of objects is found in high Galactic latitude regions ($b \geq 20°$) and as a sample, it is reasonably complete ($\sim 90\%$) in the magnitude range $13.5 \leq m_{zw} \leq 15.7$ (Hernandez-Toledo et al. 1999). The selection criteria used in assembling the CIG can be expressed by the following relations:

$$\begin{gathered} x_{1i} > 20a_i \\ 0.25a_1 < a_i < 4a_1, \end{gathered} \tag{1}$$

wherex_{1i} is the apparent separation between the candidate isolated galaxy of apparent diameter a_1 and any other neighbor galaxy of apparent diameter a_i. Under these criteria, any other galaxy of comparable size ($a_i = a_1$) should be at a distance of at least 20 times its diameter (projected on the sky) from the isolated galaxy.

Assuming a typical galaxy diameter D $\sim$ 20 kpc and a peculiar velocity relative to the Hubble flow V $\sim$ 150 km s^{-1} (Rivolo & Yahil 1981), the time required for an intruder galaxy to traverse 20 diameters is $\sim 2\times10^9$ yr. This is a first-order estimate of the time since the last equal-size galaxy-galaxy interaction for a CIG system and it suggests that CIG galaxies are reasonably isolated. It is therefore expected that only the intrinsic properties of the individual galaxies in the CIG should influence the observed photometric and morphological properties.

Karachentseva (1973) included other isolation criteria (coded as 1 and 2 in her original catalogue) depending on whether or not other galaxies, within a factor of 4 in size, were found near a 20 diameter boundary or even if a galaxy is definitely not isolated according to the CIG criteria. Less isolated galaxies account for less than 5% of our CIG sample and have been excluded from the present study.

2.2. Data Reduction

A journal of the photometric observations is given in Table 1. Column (1) gives the original catalogue number, Columns (2)-(9) give the number of frames per filter, the integration time (in seconds), and seeing conditions (in arcsec).

Table 2 reports some relevant information on the observed isolated galaxies obtained from the literature. Column (1) is the CIG catalogue number, Column (2) reports other identifications, Column (3) the apparent total B magnitude from the Lyon Extragalactic Database (LEDA), Column (4) the Hubble Type from LEDA, Column (5) the apparent total B magnitude from the Nasa Extragalactic Database (NED), Column (6) the radial velocity in km s^{-1} corrected for Virgocentric infall from LEDA.

Images were debiased, trimmed, and flat-

fielded using standard IRAF[2] procedures. First, the bias level of the CCD was subtracted from all exposures. A run of 10 bias images was obtained per night, and those were combined into a single bias frame which was then applied to the object frames. The images were flat-fielded using sky flats taken in each filter at the beginning and/or end of each night.

Photometric calibration was achieved by nightly observations of standard stars of known magnitudes from the "pg0231+051" field of stars (Landolt 1992) with a color range $-0.3 \leq (B-V) \leq 1.5$ and $-0.1 \leq (B-I) \leq 3.0$. Once the principal extinction coefficients in B, V, R and I were estimated, transformations of the instrumental magnitudes to a standard system were calculated according to the following equations:

$$\begin{aligned} B - b &= \alpha_B + \beta_B (b-v)_0 \\ V - v &= \alpha_V + \beta_V (b-v)_0 \\ R - r &= \alpha_R + \beta_R (v-r)_0 \\ I - i &= \alpha_I + \beta_I (v-r)_0, \end{aligned} \tag{2}$$

where B, V, R and I are the standard magnitudes, b, v, r and i are the instrumental (and airmass-corrected) magnitudes, and α and β are the transformation coefficients for each filter.

A constant value associated to the sky background was subtracted using an interactive procedure that allows the user to select regions on the frame free of galaxies and bright stars. Errors in determining the sky background, are, in fact, the dominant source of errors in the estimation of total magnitudes.

The most energetic cosmic-ray events were automatically masked using the COSMICRAYS task, and field stars were removed using the IMEDIT task when necessary. Within the galaxy itself, care was taken to identify superposed stars. A final step in the basic reduction involved registration of all available frames for each galaxy and in each filter to within ±0.1 pixel. This step was performed by measuring centroids for foreground stars on the images and then performing geometric transformations using GEOMAP and GEOTRAN tasks in IRAF.

2.3. Errors

Apparent magnitudes for each galaxy were estimated in three concentric circular apertures. This was achieved in $BVRI$ bands by using the PHOT routines in IRAF. Here we report the total apparent magnitudes while in the appendix we report apparent magnitudes at two other circular apertures, also in $BVRI$ bands. See Table A1.

An estimation of the errors in our photometry involves two parts: (1) The procedures to obtain instrumental magnitudes and (2) the uncertainty when such instrumental magnitudes are transformed to the standard system.

For item (1), notice that the magnitudes produced at the output of the IRAF routines (PHOT) have a small error that is internal to those procedures. Since we have also applied extinction corrections to the instrumental magnitudes in this step, our estimation of the errors are mainly concerned with these corrections and the estimation of the airmass. After a least square fitting, the associated errors with the slope for each principal extinction coefficient are: $\delta(k_B) \sim 0.02$, $\delta(k_V) \sim 0.02$, $\delta(k_R) \sim 0.02$ and $\delta(k_I) \sim 0.015$. An additional error $\delta(airmass) \sim 0.005$ from the airmass routines in IRAF was also considered.

[2]The IRAF package is written and supported by the IRAF programming group at the National Optical Astronomy Observatories (NOAO) in Tucson, Arizona. NOAO is operated by the Association of Universities for Research in Astronomy (AURA), Inc. under cooperative agreement with the National Science Foundation (NSF).

For item (2), the zero point and first order color terms are the most important to consider. After the transformation to the standard system by adopting our best–fit coefficients, the errors from the assumed relations for α were respectively 0.02, 0.04, 0.02 and 0.02 in B, V, R and I, and 0.02, 0.03, 0.02 and 0.02 for β. To estimate the total error in each band, it is necessary to propagate the errors, after considering the corresponding transformation equations. An estimate of the sky contribution is necessary for quoting the total uncertainties. This was achieved by estimating the total magnitudes for all galaxies before and after sky subtraction. Typical values $\delta(B) \sim 0.08$, $\delta(V) \sim 0.08$, $\delta(R) \sim 0.9$ and $\delta(I) \sim 0.1$ are obtained. Total typical uncertainties are 0.1, 0.12, 0.12 and 0.15 in B, V, R and I bands, respectively.

The estimated total magnitudes in this work were compared with other external estimations when available in the literature. This has been done for: 1) The standard stars and 2) The isolated spiral galaxies.

2.4. Standard Stars

For the standard stars, a comparison of our CCD magnitudes with those reported in Landolt (1992) for stars in the field of pg0231+051 and the Dipper Asterism M67 Star Cluster (Chevallier & Ilovaisky 1991) are shown in Figure 1.

Figure 1 shows no significant deviations between our CCD magnitudes and those reported for the standard stars. A linear fit to this plot indicates a $\sigma \sim 0.005$ as the typical internal error for our magnitude estimations.

2.5. Isolated Galaxies

Figure 2 shows a comparison of the estimated magnitudes for the isolated galaxies in B, V and I bands versus the available total magnitudes in the Nasa Extragalactic

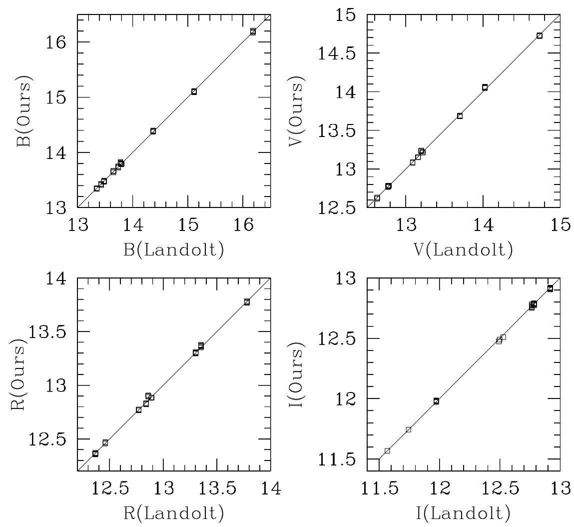

Fig. 1.— Comparison between our estimated magnitudes and those reported in Landolt (1992) for standard stars in the field of pg0231+051 and the Dipper Asterism M67 Star Cluster (Chevallier & Ilovaisky 1991).

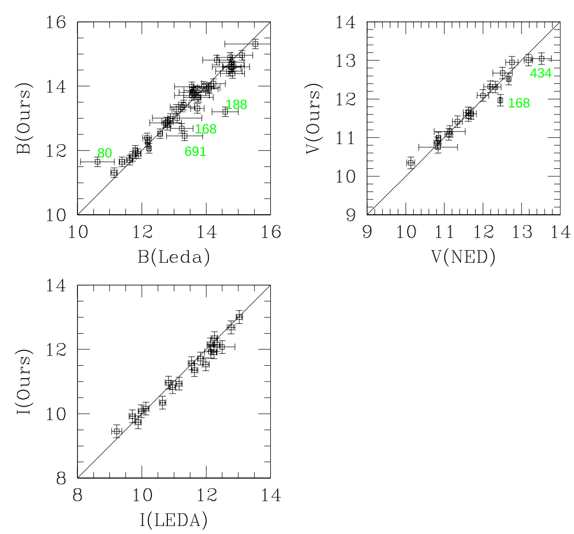

Fig. 2.— Comparison between our total B, V, R and I magnitudes and the available photometry of similar aperture from the HyperLeda Database. Discrepant cases like CIG 80, 168, 188, 434, and 691 are indicated.

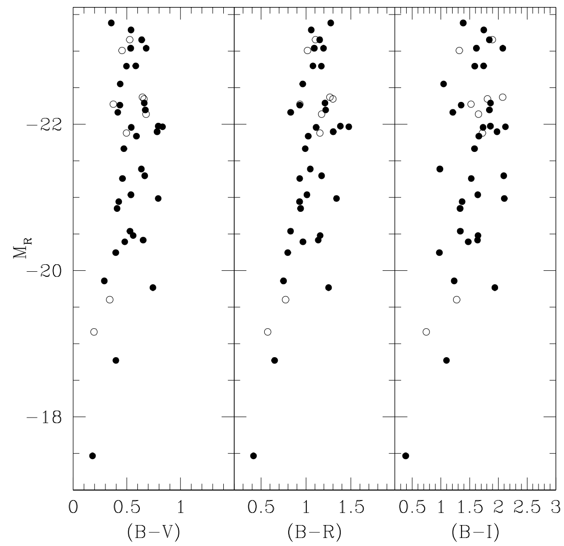

Fig. 3.— Color–magnitude diagrams for the 44 isolated spirals after galactic and internal extinction corrections. Galaxies with inclination larger than 80^o are showed with (open) circles.

Database (hereafter NED)[3] and aperture photometry in HyperLeda Databases. Discrepant cases such as CIG 80, 168, 188, 434, and 691 in the different bands are emphasized in the figure.

We find a reasonable agreement with the available values from the literature, except for a few discrepant cases shown in the Figure. HyperLeda reports detailed aperture photometry in the B-band for CIG 80. From a plot of the available data, the reported value should correspond to an aperture size log (A) $\sim$ 2 while our magnitude corresponds to log (A) = 1.58. The corresponding magnitude for an aperture similar to ours is 11.60 mag, in complete agreement with our estimation.

HyperLeda does not report any aperture photometry in the B-band for CIG 168. A detailed aperture photometry in the V and I (Cousins) bands is found instead. The V-band value in HyperLeda corresponds to log (A) = 1.44 while ours is log (A) = 1.50. An extrapolation of the available V and I magnitudes to our aperture size is consistent with our photometry. This makes us confident that our B-band value is well estimated and suggests that the B-band magnitude reported in HyperLeda should correspond to a smaller log (A) value.

In the case of CIG 188, both HyperLeda and NED databases report an homogenized magnitude from previously published data, assuming standard Johnson UBVRI filters. Notice however that NED magnitude is 14.10 $\pm$0.75 with a large error bar. Given the absence of detailed aperture photometry and the diffuse nature of this galaxy (see corresponding images below), we suggest that the observed discrepancy is explained by the different aperture sizes.

HyperLeda reports a couple of aperture data points for CIG 434 (corresponding to log (A) = 1.12 and 1.3, see Gallagher and Hunter 1986). By assuming a linear curve of growth, an extrapolation to log (A) = 1.5 (our aperture size) yields a magnitude value consis-

[3] nedwww.ipac.caltech.edu

tent with our data. NED reports an homogenized magnitude from previously published data, assuming standard Johnson UBVRI filters.

For CIG 691, HyperLeda reports a B–band magnitude of 13.33 ± 0.562 while NED reports a magnitude of 12.60 ± 0.5 which is significantly closer to our reported value. Even more, the only aperture data point in HyperLeda suggests that the reported value corresponds to a smaller aperture size than ours.

Finally, the internal accuracy of our photometry was evaluated by comparing the total magnitudes derived from individual exposures. We find RMS differences between individual measurements of $\delta(B) \sim 0.06$, $\delta(V) \sim 0.06$, $\delta(R) \sim 0.05$ and $\delta(I) \sim 0.05$. Additional magnitudes at two other concentric circular apertures in B, V, R and I for all the isolated galaxies in this study are reported in the Appendix.

3. Magnitudes and Colors

The estimated apparent magnitudes and the colors of the galaxies in the sample are presented in Table 3. Entries are as follows: Column (1) gives the CIG number; Column (2) gives the logarithmic aperture size in 0.1 arcmin units, according to the HyperLeda convention, Columns (3) to (6) give the observed integrated apparent magnitudes in B, V, R and I bands. Finally, Columns (7) to (9) give the observed $(B-V)$, $(B-R)$ and $(B-I)$ color indices. Total typical uncertainties in our photometry are 0.10, 0.12, 0.11 and 0.16 for B, V, R and I bands, respectively.

The $(B-V)$ corrected colors span the range of $0.2-1.3$ mag. This is comparable to that reported in other samples of non–interacting galaxies (e.g., de Jong 1996; Verheijen 1997). We emphasize important differences in blue Galactic absorption values between Burstein & Heiles (1982) and Schlegel et al. (1998) for CIG 103 (1.485 vs 0.440 mag), CIG 138 (1.95 vs 0.65 mag), and CIG 144 (2.135 vs 0.510 mag).

The fraction of dust seems to be larger for bigger galaxies according to empirical (e.g., Giovanelli et al. 1995; Wang & Heckman 1996; Tully et al. 1998) and theoretical (e.g., Shustov et al. 1997) arguments. Therefore, the internal extinction correction should depend not only on inclination but also on galaxy scale: $A^i_\lambda[\mathrm{mag}] = \gamma_\lambda \log(a/b)$, where a/b is the major to minor axis ratio, and γ_λ is a scale–dependent coefficient in the given passband λ. From an empirical analysis, Tully et al. (1998) inferred the coefficients γ_λ in the $BRIK$ bands as a function of the galaxy maximum circular velocity. From their data (given in Tully & Pierce 2000) we have carried out linear correlations of these coefficients with the corresponding magnitudes *not corrected* for internal extinction:

$$\begin{aligned}
\gamma_B[\mathrm{mag}] &= -6.30 - 0.40 M_B, \quad && M_B < -16.7 \\
\gamma_R[\mathrm{mag}] &= -4.20 - 0.26 M_B, \quad && M_R < -17.7 \\
\gamma_I[\mathrm{mag}] &= -3.40 - 0.20 M_I, \quad && M_I < -18.0 \\
\gamma_K[\mathrm{mag}] &= -0.85 - 0.05 M_K, \quad && M_K < -19.7. \qquad (3)
\end{aligned}$$

For values of the magnitudes larger than the limits given in eq. (3), γ_λ is assumed to be 0 (no extinction correction). For the band V, the line coefficients of γ_V were obtained by a simple interpolation of those in the bands B, R, I, and K: $\gamma_V[\mathrm{mag}] = -4.67 - 0.29 M_V$, $M_V < -17.5$. The a/b ratios estimated at the $B-25\mathrm{mag/arcsec}^2$ isophote were taken from the HyperLeda Database.

Table 4 shows foreground and internal extinction corrected color indices and absolute magnitudes. Corrections are based on data generated from the dust Galaxy maps given in Schlegel et al. (1998) and available in NED database. Entries are as follows: Column (1) gives the identification CIG number; Columns (2) to (4) give the corrected $(B-V)$, $(B-R)$ and $(B-I)$ color indices. Finally, Columns

(5) to (8) report the corrected absolute magnitudes in B, V, R and I bands. A Hubble constant value of 70 km s^{-1} Mpc^{-1} was adopted.

A more physical correction applied to the luminosities yields a B-band luminosity range ($-18.1 \leq M_B \leq -22.25$) indicating no faint spirals in this sample, except for the case of CIG 434.

In Figure 3 we plot different Color–Magnitude Diagrams [M_R vs $(B-V), (B-R)$ and $(B-I)$ colors] for our sample of isolated galaxies. There is a mild correlation of colors with magnitude, although the sample is still small. In fact, a significant dependence of color on luminosity for normal isolated disk galaxies is not expected (e.g., Avila–Reese & Firmani 2000). The dependence that several papers reported in the past was mainly due to the dependence of the internal extinction on luminosity (or circular velocity, Tully et al. 1998), which we take into account accordingly here.

4. Optical and Near-infrared (NIR) Morphology

In order to discuss the optical morphology (that could be modified by the presence of bars, rings, etc. or external factors) and its relationship to the global photometrical properties, the images for each isolated galaxy are presented in the form of a mosaic in Figure 4 including, from upper-left to lower-right panel: 1) a gray scale R-band image displayed at full intensity to look for faint external details; 2) an R band sharp/filtered image to look for internal structure in the form of star forming regions and/or structure embedded into dusty regions; the filtered/enhancing techniques (Sofue 1993) allow the subtraction of the diffuse background in a convenient way for discussing the different morphological details; 3) a $(B-I)$ color index map to visualize the spatial distribution of the SF (light–gray is for blue colors while dark–gray is for red colors); 4) a composed (sharp/filtered) NIR JHK image which is a combination of the archive J, H and $K-$band images from the Two-Micron Survey (Skrutskie et al. 2006) to complement the structural and morphological analysis; and finally, 5) the ellipticity ϵ and Position Angle PA radial profiles from the I and composed JHK images to provide evidence of the presence of bars and other structural details. (Figures 4.1 - 4.43 are available in the electronic edition of the Journal)

We identify a bar signature if the ellipticity radial profile ϵ rises to a maximum ϵ_{max} required to be above that of the outer disk, while the PA radial profile shows a plateau (within $\pm 20^o$) along the bar (Wozniak et al. 1995).

All the images are oriented according to the standard (North-East) astronomical convention. The NIR images are approximately at the same scale as the optical images. For the sake of not crowding, the major diameter (arcmin) of the optical images is specified in the caption text for each galaxy. In some cases, not all the foreground stars in each field have been removed.

We use in addition the fact that the median value of the $(B-V)$ color declines systematically as the morphological type T increases along the morphological sequence. Median integrated total $(B-V)$ colors of galaxies according to morphological class are given by Roberts & Haynes (1994). The UGC and the Local Supercluster (LSc) samples in Roberts & Haynes (1994) are rather inhomogeneous in terms of environment, but the interacting objects were excluded from their analysis. The median colors of these samples will be used as a reference in the following discussion.

4.1. Comments on Individual Objects

CIG 1. The galaxy was classified as

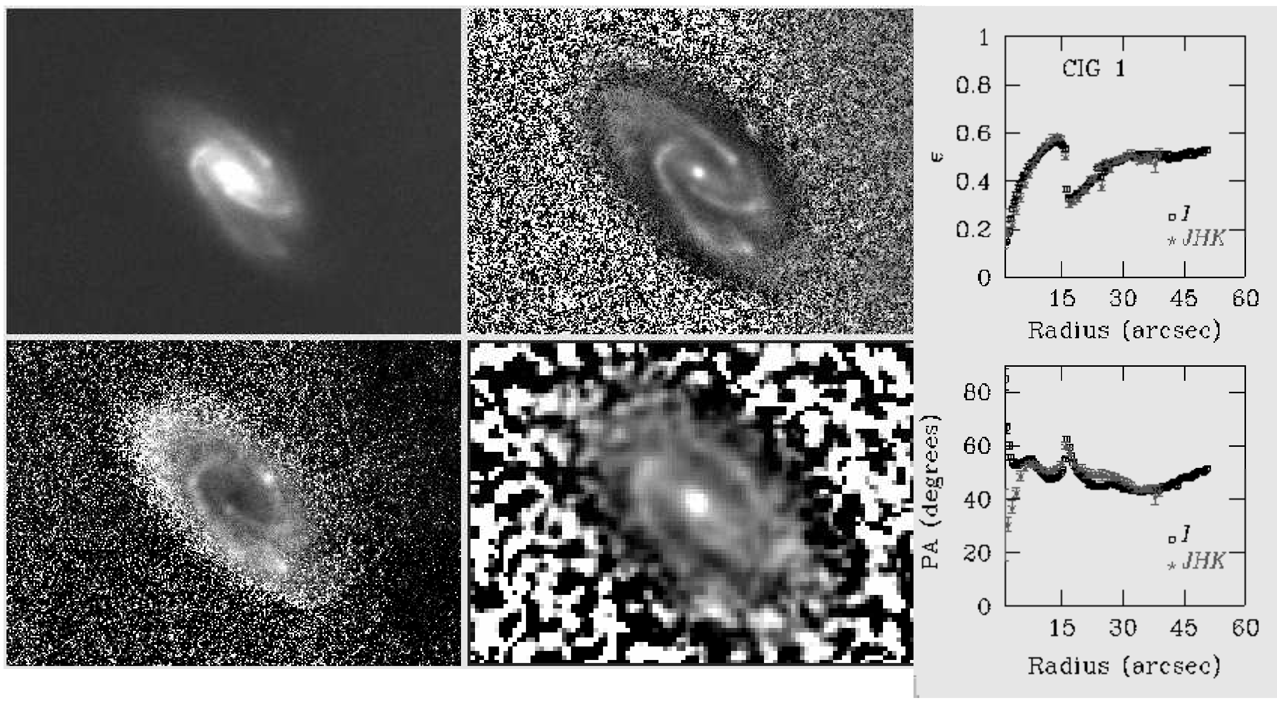

Fig. 4.— CIG 1 Mosaic (example). Upper-left:a gray scale R-band image displayed at full intensity. Upper-right: An R band sharp/filtered image. Lower-left: A $(B-I)$ color index map. Lower-right:, A composed (sharp/filtered) NIR JHK image. Right-most panel: The photometric ϵ and PA radial profiles from the I and composed JHK images. Images are oriented according to the astronomical convention. The major diameter of the galaxy in the optical images is 1.8 arcmin.

SABbc (NED). The $R-$band and sharp/filtered images show a conspicuous fan-like structure at the end of the arms resembling a tidally disturbed galaxy. The optical images show three sharp-defined arms and a bar also visible in the composed JHK image. We classify this galaxy as SBbc. The total $(B-V)$ color is representative of Sc types. The photometric I and JHK band (ϵ and PA) profiles show evidence of a bar in this galaxy.

CIG 4. The galaxy was classified as Sbc (NED). The gray-scale $R-$band image shows an inclined galaxy through a series of dust lanes. The optical R-band sharp/filtered and the $B-I$ color map images show two multiple and knotty arms and a strongly reddened central region. The composed JHK image shows two main arms and an elongated central barred-like region. We classify this galaxy as SABc. The total $(B-V)$ color is strongly reddened and not representative of Sc types. The photometric (ϵ and PA) profiles show evidence of a weak bar within the first 15 arcsec of this galaxy.

CIG 33. This galaxy was classified as SAB(rs)cd (NED). The gray-scale $R-$band image shows a faint outer arm in the east emphasizing its asymmetric appearance. Its internal s-shaped structure surrounded by a series of dust lanes and two prominent blobs in the north and south-east of the inner spiral arms are also apparent. The $B-I$ color index map shows a ring-like structure. The $JHK-$band image clearly shows an inner barred structure from which two arms emerge. We classify this galaxy as SB(rs)c. The total $(B-V)$ color is representative of Sc types. The photometric I and JHK band (ϵ and PA) profiles show evidence of a bar in this galaxy.

CIG 53. The galaxy was classified as a SB(rs)c (NED) . The gray-scale $R-$band and the sharp/filtered images show knotty features along “multiple arms, a prominent bar encircled by a ring elongated in the direction perpendicular to the bar, and the presence of strong dusty structures. The $B-I$ color map permits us to see a red central region and bluer arms. The JKH-band image confirms the barred and ringed structures and traces of the arms. We classify this galaxy as SB(r)bc. The $(B-V)$ color is representative of Sbc types. The photometric I and JHK band (ϵ and PA) profiles show evidence of a bar in this galaxy.

CIG 56. The galaxy was classified as a SB(rs)b (NED). The gray-scale $R-$band image shows a barred galaxy with two dominant arms and a third faint arm to the north-west. At the outskirts, the two arms become diffuse. The sharp/filtered image and $(B-I)$ color map show a blue ring elongated in direction of a red bar. The JHK composed image shows a prominent bar and two dominant arms. We classify this galaxy as SB(r)b. The $(B-V)$ color is representative of Sb types. The photometric I and JHK band (ϵ and PA) profiles show evidence of a bar in this galaxy.

CIG 68. The galaxy was classified as SAB(s)a (NED). The gray-scale $R-$band image shows a central elongated structure from which two arms emerge, while the sharp/filtered image shows traces of a bar. The $(B-I)$ color map shows a bluer ring elongated in direction of the bar and an adjacent dust lane. The composed JHK image shows a prominent bar and two arms. We classify this galaxy as SB(r)a. The $(B-V)$ color is representative of Sa types. The photometric I and JHK band (ϵ and PA) profiles show evidence of a bar in this galaxy.

CIG 80. The major axis of this galaxy is longer than our CCD frame. However we comment on the structure found within 4.3 arcmin. The galaxy was classified as a SA(s)b (NED). The gray-scale $R-$band and sharp/filtered images show a multi-armed and strongly asymmetric pattern enhanced by the presence of dust lanes, resembling a strongly

perturbed system. The $(B-I)$ color map shows an inner ring and bluer arms. The composed JHK image shows a barred-like structure from which two prominent arms seem to emerge and confirms the red nature of a ring oriented in the direction of the bar. We classify this galaxy as SB(r)b. The $(B-V)$ color is consistent with Sab types. The photometric (ϵ and PA) profiles show weak evidence of a bar within the first 25 arcsec of this galaxy.

CIG 103. The galaxy was classified as SAB(rs)c (NED) . This is another example of an apparently multi-armed galaxy seen through a series of strong dust lanes as shown in our $R-$band, sharp/filtered and $B-I$ color map images. The color map also shows an elongated red central region apparently encircled by a pseudo-ring alongside the direction of a bar. The composed JHK image shows evidence of a weak bar from which two arms emerge. We classify this galaxy as SB(r)c. The $(B-V)$ color is consistent with Sc types. The photometric (ϵ and PA) profiles show weak evidence of a bar or an elongated structure within the first 15 arcsec of this inclined galaxy.

CIG 116. The galaxy was classified as RSB(s)a (NED). All our images show this galaxy with two inner well-defined arms making an s-shaped structure. These arms become diffuse as they wind out, giving the appearance of an external ring oriented almost perpendicular to the bar. The internal structure is seen through strong dust lanes. The composed JHK image shows the presence of a bar and two inner dominant arms. We classify this galaxy as RSB(s)a. The $(B-V)$ color is consistent with Sa types. The photometric I and JHK band (ϵ and PA) profiles show evidence of a bar in this galaxy.

CIG 123. This galaxy is classified as SB(rs)bc (NED). From the global distribution of optical light this galaxy appears asymmetric. Our images show an apparently multiple set of faint southern arms and a strong southern dust lane. The red central region, including the bar as well as the bluer ring and arms are emphasized in the $B-I$ color index map. The composed JHK image clearly shows a strong bar, and a ring oriented in the direction of the bar. We classify this galaxy as SB(r)c. The $(B-V)$ color is consistent with Sbc types. The photometric I and JHK band (ϵ and PA) profiles show evidence of a bar in this galaxy.

CIG 138. This galaxy was classified as SB(s)d (NED). This is an inclined galaxy seen through a series of dust lanes, causing the arms to appear multiple in nature. The $B-I$ color index map clearly emphasizes the reddened nature of the light distribution. In contrast, the composed JHK image shows mainly two arms and an elongated central structure resembling a bar. We classify this galaxy as SBc. The reddened $(B-V)$ color does not correspond to ScSd types. The photometric I and JHK band (ϵ and PA) profiles do not show evidence of a bar in this galaxy.

CIG 139. The galaxy was classified as SB(s)m pec (NED). The $(B-I)$ color index map shows, however, a central reddened region and an outer bluer region similar to what is observed in spirals. There are no archive JHK images for this galaxy. We preserve NEDs classification in this case. Notice that the obtained $(B-V)$ color is representative of Sm/Irr types. The photometric I-band (ϵ and PA) profiles do not show evidence of a bar.

CIG 144. The galaxy was classified as Sb (NED). This is an edge-on galaxy showing a peanut-like-shape red bulge in the sharp/filtered image. However, the $B-I$ color index image and the composed JHK image show a different structure. We classify this galaxy as SABb. The reddened $(B-V)$ color corresponds more to Sa types. The photometric I and JHK band (ϵ and PA) profiles are consistent with the presence of a bar in

the first 30 arcsec of this inclined galaxy.

CIG 151. The galaxy was classified as SAdm (NED). This is an inclined and apparently multi-armed spiral galaxy. The central region appears elongated in the sharp/filtered image and red in the $B - I$ color map. The composed JHK image suggests a bar structure and two adjacent arms. We classify this galaxy as SABc. The $(B - V)$ color corresponds to Sc types. The photometric I and JHK band (ϵ and PA) profiles show a weak evidence of a bar in this inclined galaxy.

CIG 154. The galaxy was classified as SBcd (NED). This apparently disturbed galaxy shows an elongated and reddened central region. The winding of the inner arms suggests a ring oriented in the direction of the bar. The inner arms appear bifurcated at various places and faint outer arms are also perceived. The composed JHK image shows a bar and a ring. We classify this galaxy as SB(r)cd. The $(B - V)$ color corresponds to ScdSd types. The photometric I and JHK band (ϵ and PA) profiles show evidence of a bar in the first 10 arcsec and of a ring at about 12 arcsec in this galaxy.

CIG 168. The galaxy was classified as SAB(s)bc (NED). The galaxy appears moderately flocculent in the optical images with an elongated and red central region. The composed JHK image also suggests an elongated central structure and only two prominent arms. The $(B - V)$ color corresponds to ScdSd types. We classify this galaxy as SAB(s)cd. The photometric I and JHK band (ϵ and PA) profiles do not show evidence of a bar.

CIG 175. The galaxy was classified as SA(s)a pec (NED). The optical images show traces of diffuse and faint arm-like features and a prominent central region. The knotty appearance in the central part may be either intrinsic or caused by some coincident field stars not appearing in the composed JHK image. The $(B - V)$ color corresponds to SmIm types. We classify this galaxy as Sa pec. The photometric I and JHK band (ϵ and PA) profiles are consistent with smooth precessing arm-like features.

CIG 180. The galaxy was classified as SA(rs)c (NED). The optical images show a multiple set of tightly wound arms and a reddened central region apparently encircled by an inner ring. In contrast, the composed JHK image shows a prominent central region and traces of the adjacent disk. We classify this galaxy as SA(r)b. This is an interesting case of a non-barred spiral with a symmetric inner ring that also shows hints of a circumnuclear ring. The $(B - V)$ color corresponds to Sab types. The photometric I and JHK band (ϵ and PA) profiles show weak evidence of a central ring within the first 10 arcsec and emphasize, in contrast with the optical image, a smooth nature of the central near-IR structure in this galaxy.

CIG 188. The galaxy was classified as SAB(s)d (NED). This galaxy shows multiple arms in the optical images. The sharp/filter image allows us to see a central bar structure that is red in the $(B - I)$ color map. The low signal in the composed JHK image does not permit us to appreciate the central bar but the photometric I and JHK band (ϵ and PA) profiles confirm the presence of a central bar. The total $(B - V)$ color is representative of SdSm types. We classify this galaxy as SB(s)d.

CIG 208. The galaxy was classified as Sb (NED). This is a highly inclined galaxy. The sharp/filter and color index images show the central region resembling a long bar and the outer arms. The total $(B - V)$ color is representative of ScdSd types. The photometric I and JHK band (ϵ and PA) profiles also resemble a bar within the first 25 arcsec. We classify this galaxy as SABcd.

CIG 213. The galaxy was classified as S0

(NED). We are using the B band image to show a bar surrounded by an almost circular ring oriented in the direction of the position angle of the bar. The total $(B-V)$ color is representative of ES0 types. We classify this galaxy as RSB0. The photometric B and JHK band (ϵ and PA) profiles confirm a bar within the first 25 arcsec.

CIG 224. The galaxy was classified as SB(rs)d (NED). The optical images show a galaxy of flocculent appearance with an outer pseudo-ring and evidence of a bar. The composed JHK image is of low signal but still shows an elongated central region. The total $(B-V)$ color is representative of SdSm types. We classify this galaxy as RSBd. The photometric I and JHK band (ϵ and PA) profiles show a bar within the first 15 arcsec.

CIG 237. The galaxy was classified as Sc (NED). This is an edge-on galaxy. The total $(B-V)$ color is representative of Scd types. Based on the observed prominence of the bulge region in the optical and composed JHK images, we assume a Sc classification.

CIG 309. The galaxy was classified as SA(r)ab (NED). The optical and JHK images show an inner and outer ring. The optical images show an intermediate region of strongly wound and knotty arms?. The total $(B-V)$ color is representative of S0Sa types. We classify this galaxy as RS(r)a. The smooth behavior of the photometric I and JHK band (ϵ and PA) is consistent with an early-type galaxy.

CIG 314. The galaxy was classified as SAB(rs)c (NED). This is a multi-armed knotty spiral showing a red central region. The composed JHK image barely shows part of two arms emanating from an elongated central region. The photometric I and JHK band (ϵ and PA) profiles show evidence of a weak bar. The total $(B-V)$ color is representative of ScSd types. We classify this galaxy as SAB(rs)c.

CIG 434. The galaxy was classified as Im (NED). The optical images show a Magellanic-type irregular with an elongated and red region resembling a bar. There are no detected images available in the 2MASS survey. The total $(B-V)$ color is representative of Im types. We keep the Im classification. The photometric I and JHK band (ϵ and PA) profiles show evidence of a bar.

CIG 472. The galaxy was classified as SAB(rs)c (NED). The optical images show a pattern of two arms that become bifurcated at the outer regions. In contrast, the composed JHK image shows a single prominent northern arm extending to the south. The total $(B-V)$ color is representative of ScSd types. The photometric I and JHK band (ϵ and PA) profiles show no evidence of a bar. We classify this galaxy as SA(rs)c.

CIG 518. The galaxy was classified as SA(s)c (NED). The optical images show a pattern of two arms that become bifurcated at the outer regions and a red elongated central region. In contrast, the composed JHK image shows only two prominent arms that appear to enclose an elongated central region. The photometric I and JHK band (ϵ and PA) profiles show evidence of a bar. The total $(B-V)$ color is representative of SbSc types. We classify this galaxy as SB(s)bc.

CIG 528. The galaxy was classified as SAbc (NED). The optical images show a spiral pattern with two faint thin outer arms in the NE and SW resembling tidal tails. The composed JHK image shows only part of two central arms. The total $(B-V)$ color is representative of ScSd types. The photometric I and JHK band (ϵ and PA) profiles do not show evidence of a bar. We classify this galaxy as SA(rs)cd.

CIG 549. The galaxy was classified as SA(rs)c (NED). The optical images show a multiple set of arms while the composed JHK image shows two arms at the center and an in-

triguing feature in the SE. The total $(B-V)$ color is representative of Sbc types. The photometric I and JHK band (ϵ and PA) profiles show evidence of a bar. We classify this galaxy as SB(rs)c.

CIG 604. The galaxy was classified as (R)SB(s)a (NED). The optical images show a boxy bulge and two arms forming an outer ring. The sharp/filter and composed JHK images show enhanced emission at the starting region of the arms in the NE and SW. The photometric I and JHK band (ϵ and PA) profiles show a large scale bar. The total $(B-V)$ color is representative of Sab types. We classify this galaxy as RSB(s)a pec.

CIG 605. The galaxy was classified as SB(r)ab (NED). The optical images show multiple arms emanating from the end points of a bar. An inner ring oriented along the major axis of the bar is also appreciated. Two bright knots at the opposite sides of the bar are also seen in the composed JHK image. The total $(B-V)$ color is representative of SabSb types. We classify this galaxy as SB(r)b.

CIG 691. The galaxy was classified as SB(rs)d (NED). The optical images show a bar from which a diffuse set of arms emanates. At the composed JHK image, only the bar can be seen. The total $(B-V)$ color is representative of ScScd types. We classify this galaxy as SB(rs)cd.

CIG 710. The galaxy was classified as SA(s)cd (NED). The optical and composed JHK images show an elongated central region resembling a bar. The photometric I and JHK band (ϵ and PA) profiles also show a weak evidence of a bar. The total $(B-V)$ color is representative of SdSm types. We classify this galaxy as SB(s)cd.

CIG 889. The galaxy was classified as Sa (NED). This is an edge-on galaxy showing a prominent peanut-shaped bulge from the optical to the NIR. This shape has been interpreted as representing a barred structure seen at high inclinations (c.f. Bureau & Athanassoula 2005). We classify this galaxy as SBa. The $(B-V)$ color corresponds to Sa types. The photometric I and JHK band (ϵ and PA) profiles are consistent with the presence of a bar in the first 30 arcsec of this inclined galaxy.

CIG 906. The galaxy was classified as Sb (NED). This is an edge-on galaxy. The sharp/filtered image allow us to see a prominent dust band along the plane and the $B-I$ color index image shows this plane as highly reddened but with a bluer outer region. A bulge can be appreciated in the composed JHK image. We preserve NED classification. The $(B-V)$ color corresponds to Sab types. The photometric I and JHK band (ϵ and PA) profiles may be consistent with the presence of a bar in the first 30 arcsec of this galaxy.

CIG 910. The galaxy was classified as SBab (NED). This is another highly inclined galaxy that shows two main diffuse arms in the optical images. The sharp/filtered and $B-I$ color index images show evidence of a red barred structure and an outer bluer region. The composed NIR image confirms both the barred structure and the presence of two arms. We classify this galaxy as SBab. The $(B-V)$ color corresponds to Sa types. The photometric I and JHK band (ϵ and PA) profiles are consistent with the presence of a bar in the first 30 arcsec of this galaxy.

CIG 911. The galaxy was classified as SBb (NED). The optical images show multiple arms emanating from a central ringed region that encloses a bar. The bar is red in color while the arms are bluer. The composed JHK image permits us to see a barred structure enclosed by a ring oriented in the direction of the bar. We classify this galaxy as SB(r)b. The $(B-V)$ color corresponds to Sb types. The photometric I and JHK band

(ϵ and PA) profiles show evidence of a bar in the first 15 arcsec of this galaxy.

CIG 935. The galaxy was classified as SAB(rs)cd (NED). The optical images show a multi-arm pattern with an elongated central region. In contrast, the composed JHK image shows traces of a two-arm central pattern. The photometric I and JHK band (ϵ and PA) profiles show weak evidence of a bar. The $(B-V)$ color corresponds to SbcSc types. We classify this galaxy as SAB(rs)c.

CIG 976. The galaxy was classified as Sab (NED). The optical images show an apparently disturbed spiral pattern while the composed JHK image shows only a two-arm pattern. The photometric I and JHK band (ϵ and PA) profiles do not show evidence of a bar. The $(B-V)$ color corresponds to SabSb types. We classify this galaxy as SA(s)ab.

CIG 983. The galaxy was classified as SAB(rs)c (NED). The optical images show a multi-armed spiral pattern with a slightly elongated central region. The sharp/filter image shows only a two-arm pattern and also a slightly elongated central region. The photometric I and JHK band (ϵ and PA) profiles show weak evidence of a bar. The $(B-V)$ color corresponds to ScdSd types. We classify this galaxy as SB(rs)cd.

CIG 1004. The galaxy was classified as SB(s)c (NED). The optical images show a bar and a multi-armed spiral pattern. The composed JHK image shows only a two-arm spiral pattern and a prominent large-scale bar. The photometric I and JHK band (ϵ and PA) profiles also show evidence of a large bar. The $(B-V)$ color corresponds to SbcSc types. We classify this galaxy as SB(s)c.

CIG 1009. The galaxy was classified as Sa (NED). The optical images show a set of tightly wound arms forming an inner ring. The composed JHK image also shows a central arm pattern. The photometric I and JHK band (ϵ and PA) profiles do not show evidence of a bar. The $(B-V)$ color corresponds to SabSb types. We classify this galaxy as S(r)ab.

CIG 1023. The galaxy was classified as SB(r)b (NED). The optical images show arms forming an outer ring. A bar is seen enclosed by an inner ring alongside the major axis of the bar. The arms appear to start at the end parts of the bar. The composed JHK image shows prominence of the bar. The $(B-V)$ color corresponds to SabSb types. We classify this galaxy as RSB(r)b.

4.2. Generalities of the sample

Table 5 is a summary of the morphological results found in this work. Column (1) gives the original catalogue number, Column (2) gives the Hubble Type as reported in NED, Column (3) gives the Hubble Type as estimated in this work, Column (4) remarks the presence of Bars/Rings, Column (5) remarks the presence of multiple arms from the optical ($BVRI$) images, and Column (6) reports the Bar ellipticity (corrected for inclination).

NED database contains morphological information on subtypes for almost all these isolated galaxies, except for some of the most inclined ones (CIG 144, 208, 237, 889 and 906). 42% of the galaxy sample is earlier than Sbc and 52% is of Sbc type or later. The catalogue information concerning bars (confirmed and presumed) comprised 27 galaxies before this work, and we were able to add this information to 8 other galaxies. This indicates that up to 79.5% of the isolated galaxies in this subsample shows evidence of barred structure: for 63.5% the evidence is clear (SB galaxies) and for 16% the bars are weak or suspected (SAB galaxies). The bar fraction is roughly the same for early and late types. We have measured the $I-$band and JHK isophotal ellipticities associated with a bar and calculated the maximum ellipticity, $\epsilon_{\rm max}$. This

quantity (corrected by inclination) is related to a measure of the bar strength such as the gravitational bar torque (Laurikainen et al. 2002). Column 6 in Table 5 gives the values of $\epsilon_{\max}$ for our sample. Among barred galaxies, the average value of $\epsilon_{\max}$ is 0.39 ± 0.1. If we include the values of $\epsilon_{\max} = 0.39$, 7 early type galaxies and 6 late type galaxies have $\epsilon_{\max} \geq 0.4$, which is commonly considered as evidence of strong bar. Similarly, the catalogue information for rings in our sample comprised before 16 galaxies; in this work, it has been added to 8 other galaxies, accounting now to 55% of the sample.

Finally, we emphasize the finding of clear morphological signatures of disturbance at least in two galaxies, CIG1 and CIG80. The disturbance is revealed in the former case by a broad fan–like shape of the outer arms, while in the latter case it is revealed by a strong global asymmetric pattern of the multi–arms (see Figs. 4 and 10, and §§4.1).

5. Physical Morphology

Physical morphology has appeared as an alternative to classifying galaxies on the basis of physical properties rather than on visual features (see Morgan & Osterbrock 1969; Abraham et al. 1996; Conselice 1997; Bershady, Jangren & Conselice 2000, among others). Conselice (2003, and more references therein) has provided a useful framework for classifying galaxies closely tied to underlying physical processes and properties. Conselice (2003; hereafter C2003) argues that the major ongoing and past formation modes of galaxies can be distinguished using three model–independent structural (photometric) parameters, which allow for a robust classification system. These parameters are the concentration of stellar light (C), its asymmetric distribution (A), and a measure of its clumpiness (S).

Below we present below the CAS parameters measured at various passbands for our observed sample of isolated galaxies. The CAS characterization of this set of isolated galaxies is also helpful as a comparative sample for interpreting similar results of other surveys that sample galaxies in a wide range of environments (e.g., C2003; Hernandez–Toledo et al. 2005; 2006). Next, we briefly review each one of the CAS parameters.

Concentration of light C.- The concentration index C is defined as the ratio of the 80% to 20% curve of growth radii (r_{80}, r_{20}), within 1.5 times the Petrosian inverted radius at r($\eta = 0.2$) (r'_P) normalized by a logarithm: $C = 5 \times log(r_{80\%}/r_{20\%})$ (see for more details C2003). The concentration is related to the galaxy light (or stellar mass) distributions.

Asymmetry A.- The asymmetry index is the number computed when a galaxy is rotated 180° from its center and then subtracted from its pre-rotated image, and the summation of the intensities of the absolute value residuals of this subtraction is compared with the original galaxy flux (see for more details C2003). This parameter is also measured within $1.5 \times r'_P$. The A index is sensitive to any feature that produces asymmetric light distributions. This includes galaxy interactions/mergers, large star-forming regions, and projection effects such as dust lanes (Conselice 1997; Conselice et al. 2000).

Clumpiness S.- Galaxies undergoing SF are very patchy and contain large amounts of light at high spatial frequency. To quantify this, the clumpiness index S is defined as the ratio of the amount of light contained in high frequency structures to the total amount of light in the galaxy within $1.5 \times r'_P$ (C2003). The S parameter, because of its morphological nature, is sensitive to dust lanes and inclination (C2003).

Measurement of CAS *parameters*.- The measurement of the CAS parameters for the

isolated spiral galaxies was carried out in several steps:

(i) close field and overlapping stars were removed from each image; (ii) sky background was removed from the images; (iii) the center of each galaxy was considered as the barycenter of the light distribution and the starting point for measurements; (iv) the CAS parameters for all the spiral isolated galaxies were estimated directly, i.e. isolated galaxies are not influenced by light contamination from any other galaxy of similar size in the neighborhood (isolation criteria); (v) galaxies with high inclinations or axis ratios could introduce systematic biased trends in the values of the CAS parameters (C2003). Isolated galaxies whose apparent axial ratios yield "inclinations" larger than 80° are represented as open circles on the corresponding plots.

5.1. CAS Results

Since CAS parameters are mostly reported in the R band by other authors, in order to compare, we provide here the calculated CAS parameters and their errors, also in the R band (Table 6). The CAS values in the other bands for our observed isolated spirals will be provided by the authors upon request.

By sorting the sample in early– and late–type spirals (SaSb and SbcSm, respectively), the corresponding average and standard deviation values of the CAS parameters are: $< C(R) > (SaSb) = 4.00 \pm 0.50$, $< A(R) > (SaSb) = 0.08 \pm 0.05$, $< S(R) > (SaSb) = 0.20 \pm 0.12$, and $< C(R) > (SbcSm) = 3.10 \pm 0.40$, $< A(R) > (SbcSm) = 0.19 \pm 0.10$, $< S(R) > (SbcSm) = 0.36 \pm 0.20$. Our mean values are consistent with those reported in C2003 for the Frei et al. (1996) sample of non–interacting galaxies, except in the case of $< S(R) >$ (SbcSm). Notice however that irregulars were included in in SbcSm class while in C2003 these galaxies are separated.

An interesting question is how the CAS parameters do change with wavelength. Figure 5 shows the cumulative distribution function of the CAS parameters at B, R, J and K bands. This comparison let us see visually that there are significant systematic changes in the CAS parameters with wavelength. The concentration C becomes higher from bluer to redder bands, specially for those galaxies with low and intermediate values of C. In the case of both the asymmetry A and clumpiness S parameters, their values strongly decrease from bluer to redder bands, more as larger are these parameters.

In Figure 6 we plot the average and standard deviation values of the CAS parameters vs wavelength (color band) for our sample sorted in early– and late–type spirals (SaSb –left panel– and SbcSm –right panel, respectively). The CAS parameters of later types show on average more dependence (and scatter) with wavelength than the early types. Among the CAS parameters, the clumpiness is the most sensitive to wavelength.

6. Discussion

6.1. Morphology, Bars, and Rings in Isolated Galaxies

The optical and IR emission in galaxies are dominated by different populations of stars and are subject to dust absorption at different levels. The structures that are dominated by older stellar populations are more prominent and less affected by extinction in the IR than in the optical. In the IR one observes a higher bar fraction than in the optical, as well as cases where the bulge appears more prominent, the spiral arms less flocculent and rings less prominent (Eskridge et al. 2000). The latter points towards an earlier–type classification from the IR images than from optical ones. The same trends mentioned above are observed for our sample of isolated galaxies.

It should be remarked that, in our attempt to describe the morphology of the observed galaxies, we also have made use of the JHK images from the the Two Micron-Survey.

The re–classification presented here (see Table 5) preserves the optically observed morphology but takes into account the NIR bar morphology. In general, previous results concerning the differences in morphology as passing from optical to NIR bands (Eskridge et al. 2000) agree with the ones seen in our subsample of isolated galaxies, though the fraction of isolated galaxies for which these differences become significant is actually small in our case ($\sim 15\%$).

Concerning bars in our isolated galaxies, they come into a variety of sizes, shapes and color distributions; from apparently strong, to small ones confined to the central parts of galaxies and up to the oval-shaped bulges, suggesting a range of strengths, lengths and mass distributions. We have shown that the fraction of galaxies in our sample with clear evidence of optical/IR bars (SB galaxies) is 63%, while 16% more show some evidence of weak bars (SAB galaxies). These fractions are in agreement with estimates from larger samples of galaxies. For example, Eskridge et al. (2000) determined the fraction of strongly barred galaxies in the $H-$band for a sample of 186 spirals *from different environments* to be 56%, while another 16% is weakly barred. For the same sample, the fraction of barred galaxies reported in the optical is almost a factor of two smaller than in the NIR. We do not find such a strong difference with the passband in our sample of isolated galaxies. We also reported the presence of inner (r) and outer (R) rings when possible, but a detailed ring morphology (Buta 1986; 1995) was not attempted. The fraction of galaxies with rings in our sample is high, 55%.

Notice that the observed fraction of bars and rings in the present paper can hardly be a bias of our observing procedure since we simply selected objects according to their availability in the sky.

The high fractions of bars for the isolated galaxies found here, similar to the fractions observed in other environments, could be suggesting that interactions and the global effects of the group/cluster environment are not crucial for the formation/destruction of bars. How do bars form in isolated environments? It is known that the presence and evolution of bars in a Hubble time depends on the host galaxy structure, the dark matter halo structure, the disk-to-halo ratio, as well as on the environment (e.g., Athanassoula 2003; Berentzen, Shlosman & Jogee 2006; Colín et al. 2006). High–resolution N-body simulations of isolated disks embedded in CDM halos show that extended strong bars form almost always, but they slow down as a result of angular momentum transport to the disk and halo (Debattista & Sellwood 2000; Athanassoula & Misiriotis 2002; Valenzuela & Klypin 2003); eventually, the bars may dissolve forming a pseudobulge (e.g., Avila-Reese et al. 2005; Berentzen et al. 2006).

The isolated environment may be ensuring the presence of dynamically cold disks that can form a variety of stellar bars. The observed bar fraction could also be a consequence of long–lived bars, or alternatively, of bars that recurrently form, self–destroy, and resurrect due to gas accretion (Bournaud & Combes 2002). Constant gas accretion is a condition more viable in isolated environments than in group/clusters.

Our data reveal no difference in the relative bar fraction of early– (SaSb) and late– (SbcSm) type galaxies. If any, among the barred galaxies, the late–type subsample contains a larger fraction of weakly barred (SAB) galaxies than the early–type subsample. Eskridge et al. (2000) also found that the fraction of barred galaxies almost does not depend

on morphological type. It seems that rather than the fractions, the properties of the bars (length, strength, surface brightness profile, etc.) are those that change as a function of the morphology and/or environment (e.g., Erwin 2005 and references therein). For our sample, we have estimated the bar deprojected maximum ellipticity, $\epsilon_{\max}$. We do not find significant differences in $\epsilon_{\max}$ as a function of morphological type as well as a function of the CAS parameters. Further analysis is necessary to infer the disk and bar properties and compare them with model predictions.

Another relevant topic is that of ring formation in isolated environments. Rings of SF are a common phenomenon in disk galaxies. Most rings form by gas accumulation at resonances, usually under the continuous action of gravity torques from a bar pattern, but sometimes in response to a mild tidal interaction with a nearby companion (Buta & Combes 1996; Buta 1999). In either case a resonance is a very special place in a galaxy where SF can be enhanced and may proceed either as a starburst or continuously over a period of time. Most of the observed rings in our galaxies are of the type encircling the end of the bars and elongated along the bar's position angle. Singular cases of outer rings, inner rings and a probable circumnuclear ring were detected. Contrary to bars, most of the observed rings in these isolated galaxies show bluer color distributions suggesting that their stellar populations are more similar to those in their hosting disks than those in the bars. However, some of our composed JHK images also show the prevalence of the rings in the NIR. The existence of this old population rings underlying star forming rings suggest a strong coupling between the stellar and gaseous components in the resonance regions.

Finally, it should be mentioned that in any of the 44 isolated galaxies studied here, we did not find strong signatures of interactions or perturbations. However, in two cases (CIG1 and CIG80) moderate morphological distortions can be seen, which could evidence some level of dynamical disturbance, though, these distortions could hardly be produced by strong interactions, as is the case of the isolated disturbed galaxies reported in Karachentsev et al. (2006, see Introduction). Satellite accretion could explain the distortions seen in CIG1 and CIG80. On the other hand, as mentioned above, bars and rings are axi–symmetric structures that can be explained as a product of the internal secular evolution of disks. Interactions and perturbations may induce and amplify bar/ring formation but can also contribute to their fast dissolution. A larger sample is necessary in order to explore whether or not a fraction of isolated galaxies shows evident signatures of interaction, a question of relevance as mentioned in the Introduction.

6.2. Physical Morphology through the CAS parameters

Light concentration, asymmetry and clumpiness CAS parameters have been used in alternative galaxy classification schemes (see for references §5). The CAS parameters allow also the possibility to classify galaxies according to their interaction state (C2003; Hernández–Toledo et al. 2005,2006), which is useful in high–redshift studies. In this sense, it is important to have a well studied 'comparative' sample of local isolated galaxies. In spite of the small number of galaxies in our current sample, we will introduce below an indicative discussion of the measured CAS parameters in different color bands and of their trends with other galaxy properties.

Figure 7 shows the loci of the isolated SaSb and SbcSm galaxies in the projected planes of the $R-$band CAS space. Only the averages and their standard deviations are shown (crosses and continuous error bars). The

boxes indicate the amplitude of variation of the CAS parameters (lower and upper limits) from B, V, R, I, J to K bands. For comparison, the $R-$band averages and standard deviations of galaxies in interacting S+S pairs (Hernández–Toledo et al. 2005), and starburst and Ultra Luminous Infrared (ULIR) galaxies (C2003) are also plotted. Visually, the major difference between isolated spirals and interacting, starburst and ULIR spirals takes place in the $A-S$ plane.

6.2.1. Concentration

The quantitative measure of C in our isolated spirals span the range $3.0 \leq C(R) \leq 4.5$, in agreement with other works. The average and standard deviation values are $< C(R) >= 3.5 \pm 0.59$. It is known that for lenticular and elliptical galaxies, the concentrations are typically larger than for spirals (e.g., C2003; Hernández–Toledo et al. 2006). We have also found that C systematically increases with the passband for almost each one of the isolated galaxies (Fig. 5). This is in agreement with previous finds that the scalelength of spirals is smaller in NIR bands than in the optical ones (e.g., de Jong 1996), which is probably pointing out probably to an inside–out galaxy formation scenario: bluer colors trace younger stellar populations, and if the disk is more extended in the optical than in the NIR, then the outer disk might be younger (more recently assembled) than inner regions. Metallicity gradients would emulate such an effect, but it seems that this is not the case (de Jong 1996).

According to our current understanding of galaxy formation, disks form generically inside–out within growing CDM halos (see for a recent review Avila–Reese 2006). Their concentrations (or surface brightnesses) depend mainly on the spin parameter of the halo. CDM halos span a wide lognormal distribution of the spin parameter, hence, one expects

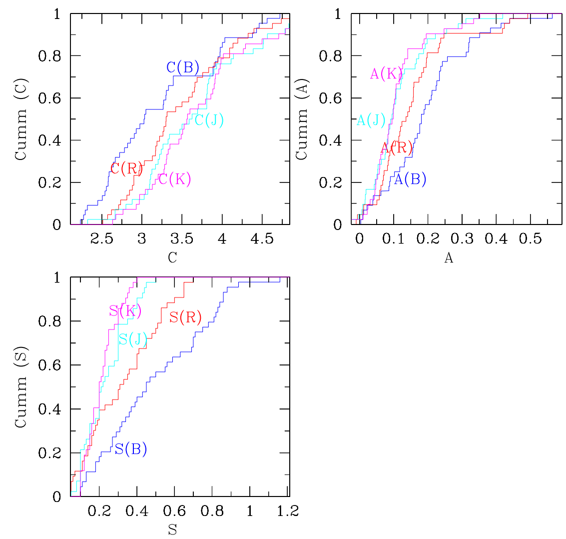

Fig. 5.— Cumulative distribution function of CAS parameters in the bands B, R, J and K bands.

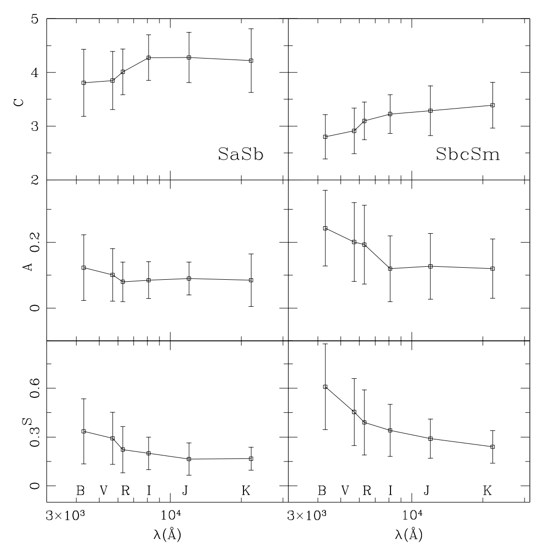

Fig. 6.— Average and standard deviation values of the CAS parameters as a function of the central wavelength $\lambda(\AA)$. Left and right columns are for the subsamples of early (SaSbc) and late (ScSm) isolated galaxies.

also a wide range of concentrations for the disks. Probably, the observed distribution of concentrations for isolated disk galaxies is not as wide as we would expect from theory. It should be also taken into account that internal secular processes after disk formation rearrange the mass (light) distribution, and that the presence of a large bulge in early–type spirals tends to increase their C parameter with respect to galaxies with smaller bulges. A fair comparison of concentrations observed in isolated spirals with model predictions is certainly a promising avenue of research. In the cases of ellipticals (and probably the bulges of early–type galaxies), theory suggests that they are more concentrated due to the violent and dissipative processes that are at the basis of their formation: major mergers of gaseous disks.

Concentration of light has been shown to correlate with properties of galaxies like Hubble type, color, and surface brightness (Okamura et al. 1984; C2003; see below). More recent studies have also shown that concentration of light correlates with internal scaling properties such as velocity dispersion, size, luminosity, and black hole mass (Graham et al. 2001).

6.2.2. Asymmetry

Concerning asymmetry, the method used here gives a simple quantitative measure of how a galaxy deviates from axi–symmetry. The asymmetry parameter A has been shown to be sensitive mainly to galaxy interactions/mergers, but also is influenced by SF clumps, dust lanes, and projection effects. The quantitative measure of A in the present sample of isolated galaxies spans roughly the range $0.0 \leq A(R) \leq 0.23$, the average and standard deviation being $< A(R) >= 0.15 \pm 0.10$. The later types are slightly more asymmetric on average than the earlier ones. The asymmetries reported here are definitively lower than the typical ones of interacting disk galaxies (see Fig. 7). The A parameter decreases significantly as the passband is redder (Fig. 5). For interacting spirals, the same trend was observed, but in a much less extent (Hernández–Toledo et al. 2005). This suggests that while the (high) asymmetry in interacting spirals is mainly of global/external origin –hence is more or less the same in different bands–, in the case of isolated spirals the (low) asymmetry is in part related to SF effects; this is why A is so sensitive to the passband in which it is measured. The question of whether a disk of a spiral galaxy is intrinsically asymmetric or not is of great interest. Some studies have shown that important deviations from axisymmetry exist in the optical and other wavelengths (Rix & Zaritsky 1995; Richter & Sancisi 1994; C2003). However, systematic attempts to quantify asymmetry and other measures like the CAS parameters in several wavelengths for well–selected local samples of galaxies are either rare or missing in the literature.

6.2.3. Clumpiness

Galaxies undergoing SF are patchy, specially in the bluer bands, and an important fraction of light must be in high spatial frequency structures. This is quantified through the clumpiness S parameter. For our sample of isolated galaxies, $S(R)$ ranges roughly from 0.0 to 0.6, being the average and standard deviation values $< S(R) >= 0.31 \pm 0.15$. The S parameter is on average larger and more scattered in later types than in the earlier ones as is seen in Fig. 7 (see also below). It is well known indeed that late type galaxies present more current SF activity than the early type ones. Although, the parameter S in our isolated galaxies is typically smaller than in interacting spirals, the differences are actually small, ant not so significant as in the case of the asymmetry parameter (Fig. 7). It is also

interesting to note that the increase of the S value as the passband is bluer in our isolated galaxies (Fig. 5) is much more significant than in the case of interacting galaxies (Hernández–Toledo et al. 2005).

6.2.4. Correlations

We next explore how the CAS parameters of isolated galaxies correlate with other properties and whether these correlations are sensitive to the passband or not. Figures 8 and 9 show the B, R, J and K band CAS parameters vs morphological type T and corrected total $(B-I)$ color. Nearly edge–on galaxies (inclination $\geq 80^{o}$) are plotted with (open) circles. Given that A and S are particularly sensitive to projection effects, it is important to visualize these galaxies since they may be masking any trend.

After a visual inspection of Figs. 8 and 9, the general conclusion is that any potential trend of the CAS parameters with T and total $(B-I)$ color tends typically to be more robust in the redder bands. This emphasizes the merits of IR parameters, which are less contaminated from (transient) SF effects and better represent the basic structure of galaxies. We should note that the scatters in these trends, even for the $J-$ band, are large. The images from the Two–Micron Survey are unfortunately of low quality, specially in the $K-$band. Besides, for several of our galaxies, there are not images in this Survey. Therefore, the J and K band data discussed here should be taken only as indicative ones.

Larger samples are needed in order to quantify better the showed dependences in Figs. 8 and 9, and infer from them clues to the physics of disk galaxies. Notwithstanding this, we present below a brief discussions on the observed trends.

According to Figs. 8 and 9, while the concentration tends to be higher for earlier–type and redder galaxies, the asymmetry and clumpiness tend to become smaller. The morphological type is led mainly by the bulge–to–disk ratio. The global color is also affected by this ratio. Therefore, it is expected that earlier types be more concentrated and redder. However, the C parameter and the global color are not too sensitive to the bulge–to–disk ratio for galaxies with intermediate-to-small values of this ratio (say Sb types and latter); therefore, in these cases, the measured C and global color reflect mostly the pure disk concentration and color. Thus, that C depends on T for late types, implies mainly a connection between the spiral arm properties and the disk concentration. The dependence of C on color would imply mainly that less concentrated disks have a more constant SF history, probably because their gas surface densities are low.

Concerning asymmetry, the observed dependence on T indicates that most of the asymmetry of our isolated spirals is associated with the natural flocculency in later-type galaxies as well with SF, which is more active for later types (as is evidenced also by the trend of higher S values as the types are later and the colors bluer, see above). In this interpretation, the effect of large–scale perturbations (c.f. interactions) is neglected. The A parameter could be used as a first–approximation indicator of interaction signatures in isolated spirals. An automatic analysis of images in large samples of galaxies provides easily the A parameter. An even more reliable test for interactions would be to produce the loci of the studied isolated spirals in the $A-S$ diagram, where maximum differences between isolated and interacting galaxies are revealed as was seen above (Fig 8; see also Hernández–Toledo et al. 2005). The adding of color information is also valuable as evidenced by Fig 9.

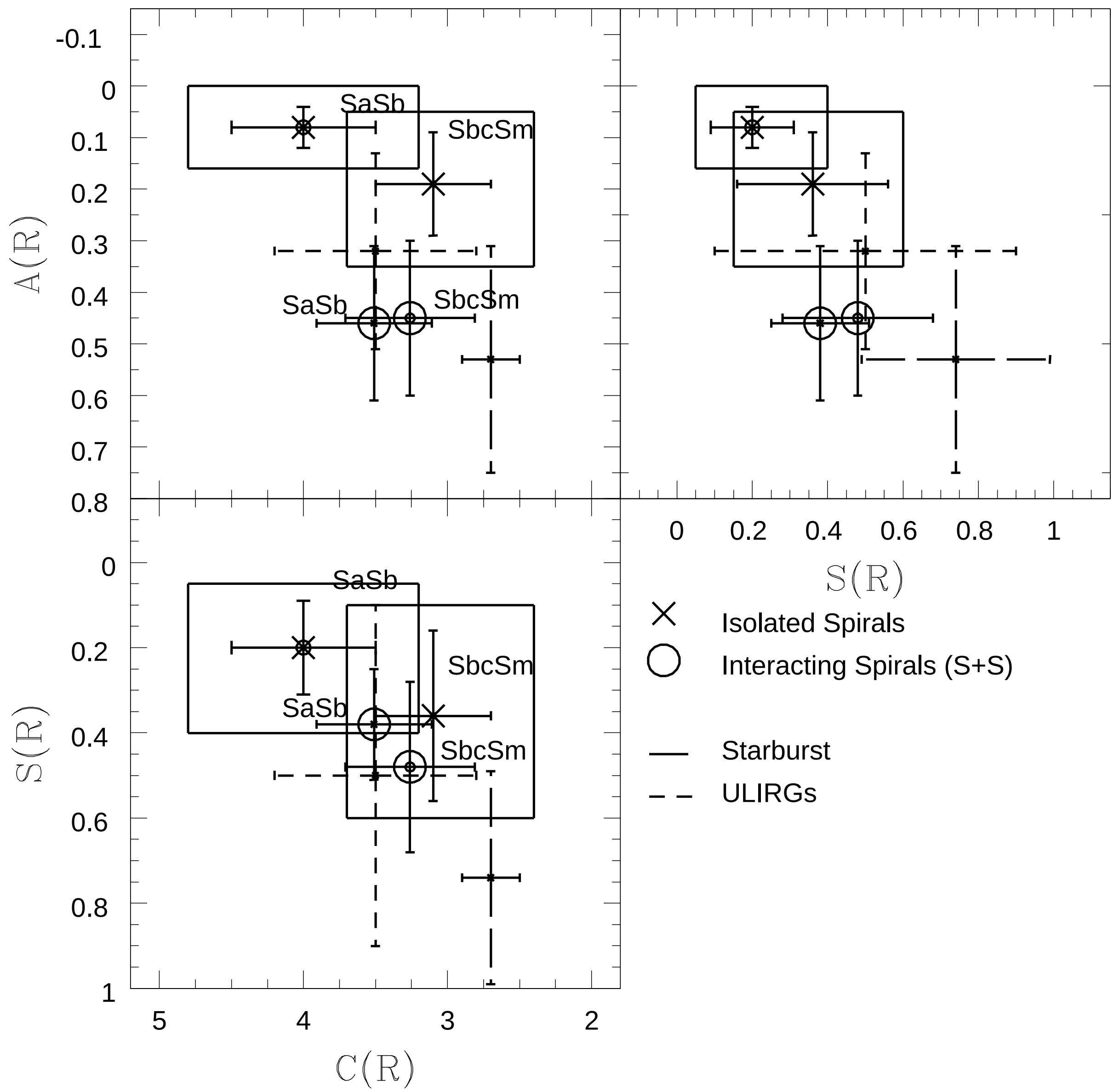

Fig. 7.— Loci of the mean $R-$band CAS values and their 1σ dispersion for our isolated SaSb and SbcSm galaxies in the CAS planes (crosses with error bars). The large boxes illustrate the amplitude of variation of the CAS values from all the bands (B, V, R, I to J and K). The corresponding $R-$band values for the interacting SaSb and SbcSm galaxies are shown with circles and solid error bars. (Hernandez–Toledo et al. 2005). Short–dashed and long–dashed error bars are for ULIR and starburst galaxies, respectively (C2003).

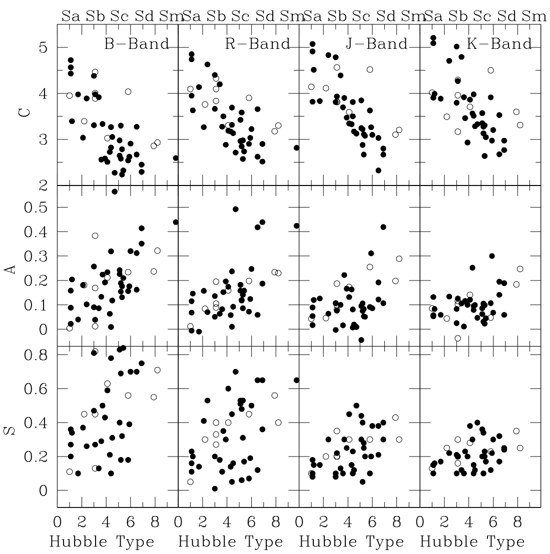

Fig. 8.— CAS parameters in the B, R, J and K bands versus the Hubble type. Galaxies with inclination larger than 80° are showed with (open) circles.

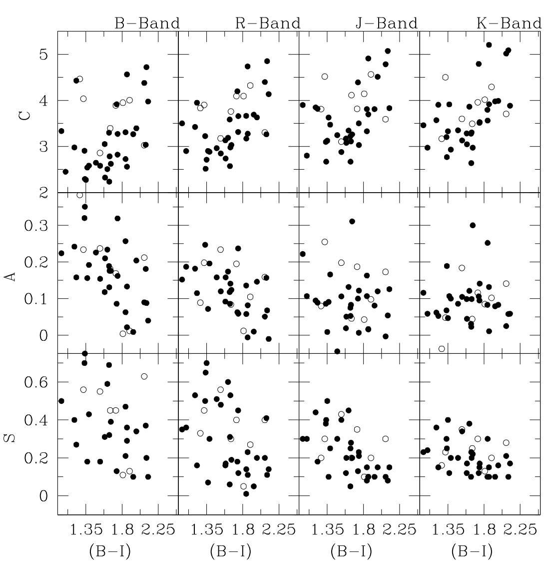

Fig. 9.— CAS parameters in the B, R, J and K bands versus the corrected total $(B-I)$ color. Galaxies with inclination larger than 80° are showed with (open) circles.

7. Summary and Conclusions

We present results of our $BVRI$ CCD photometry for a set of 44 isolated galaxies selected from the CIG catalogue (Karachentseva 1973). We have shown that our derived parameters are generally in good agreement with the aperture photometry reported in the HyperLeda database and other individual photometric works. In addition, we present multi-aperture photometry (Appendix) in order to facilitate further comparisons and contribute to the existing databases of aperture photometry (e.g., HyperLeda).

In a further step, we have analyzed the morphology of each one of the galaxies based on our mosaic $R-$band, sharp/filtered R band images, 2D $(B-I)$ color maps, composed NIR JHK images from the Two–Micron Survey archives and photometric ϵ and PA radial profiles. A morphological re–classification of the galaxies has been presented with emphasis on structural features as bars and rings and global disturbances.

The sample morphological types range from Sa to Sm, half of the galaxies being earlier than Sbc (SaSb), and the other half being Sbc or later (SbcSm). After our reclassification, we have found that $\sim$ 63% of the galaxies is clearly barred (SB), while a $\sim$ 17% more shows some evidence of a weak bar (SAB). There is not any significant difference of the bar fraction with the morphological type. The average and standard deviation values of the $I-$band deprojected maximum ellipticity of the bars, $\epsilon_{\rm max}$, is 0.39±0.1. There is not any trend of $\epsilon_{\rm max}$ with the morphological type and the CAS parameters. We have also found that 55% of the isolated galaxies in our sample shows ring structures.

Finally, we have calculated the $BVRI$, J and $K-$ band concentration, asymmetry, and clumpiness (CAS) parameters for the sample. The CAS averages and standard de-

viations in the $R-$band for the SaSb and SbcSm subsamples are: $< C(R) > (SaSb) = 4.00\pm0.50$, $< A(R) > (SaSb) = 0.08\pm0.05$, $< S(R) > (SaSb) = 0.20 \pm 0.10$ and $< C(R) > (SbcSm) = 3.10\pm0.50$, $< A(R) > (SbcSm) = 0.19\pm0.10$, $< S(R) > (SbcSm) = 0.35\pm0.20$, respectively. These values are in good agreement with previous results for non–interacting galaxies.

While C systematically increases from bluer to redder bands, both A and S significantly decrease. The CAS parameters present more robust trends with the morphological type T and the total $(B - I)$ color in the redder bands, suggesting that the basic structure of galaxies is revealed better in the IR and NIR bands. The C parameter tends to be higher for earlier–type and redder galaxies, while A and S tend to become smaller. The A parameter could be an excellent way to detect candidates to isolated spirals with signs of interaction by means of an automatic analysis of images.

The loci of our isolated galaxies in the projected planes of the CAS space depend on the morphological type (and on the color). The major difference between the isolated and interacting, starburst and ULIR spirals takes place in the $A - S$ plane.

After the completion of this paper, a work by Taylor-Mager et al. (2007) with some aims and results similar to those presented here was posted in the arXiv database. Taylor-Mager et al. analyzed the CAS parameters for a sample of galaxies (mainly late-types including peculiars) as a function of wavelength, from UV to IR $(0.15 - -0.85\mu\mathrm{m})$, with the aim of exploring how the galaxy's appearance changes with rest–frame wavelength. The result leads to a measure of the morphological k–correction for high–redshift galaxies. Their results complement well the ones presented here and both are in qualitative agreement, where comparison is possible. The building of well–defined samples of local isolated galaxies with uniform and detailed photometric information is of great relevance because it provides a fair database for comparison with model predictions as well as with observed samples of galaxies in other environments and at higher redshifts. In this paper we present a first step in the building of such a sample and discuss some preliminary results.

H.M.H.T. thanks the staff of the Observatorio Astronómico Nacional in San Pedro Mártir, B. C. for the help with the observation runs. We are grateful to the referee, Dr. Michael S. Vogeley, for his comments that improved the presentation of the paper. This work was funded by CONACYT grant 42810 to H.M.H.T. This research has made use of the NASA/IPAC Extragalactic Database (NED) which is operated by the Jet Propulsion Laboratory, California Institute of Technology, under contract with the National Aeronautics and Space Administration. This publication makes use of data products from the Two Micron All Sky Survey, which is a joint project of the University of Massachusetts and the Infrared Processing and Analysis Center/California Institute of Technology, funded by the National Aeronautics and Space Administration and the National Science Foundation. We acknowledge the usage of the HyperLeda database (http://leda.univ-lyon1.fr).

A. Aperture Photometry

Since the birth of galaxy photometry (Whitford (1936), the amount of photometric data has increased exponentially (Prugniel 1987). However, these data are inhomogeneous both in quality and format: photographic, photoelectric or more recently, CCD observations. The data are usually presented as centered aperture photometry through circular or elliptical apertures or as photometric profiles. In order to take into account the continuously growing amount of photometric data and at the same time, to make different photometric data reports somehow comparable, we present in Table A1 our estimations of integrated magnitudes in two additional concentric circular apertures. Columns (2) and (3) give the logarithm of the aperture radius (in units of 0.1 arcmin see HyperLeda convention) for each isolated spiral galaxy. Columns (4)-(11) give their corresponding magnitudes in B, V, R and I bands, respectively. The contribution of the sky to the errors in the magnitudes is relatively small at these apertures. Typical uncertainties in the magnitudes are 0.11, 0.12, 0.11 and 0.12 in B, V, R and I bands, respectively.

REFERENCES

Abraham, R. G., Tanvir, N. R., Santiago, B. X., Ellis, R. S., Glazebrook, K., & van den Bergh, S. 1996, MNRAS, 279, L47

All06 Allam, S. S., Tucker, D. L., Lee, B. C., & Smith, J. A. 2005, AJ, 129, 2062

Athanassoula E., 2003, MNRAS, 341, 1179

Athanassoula, E., Misiriotis, A. 2002, MNRAS, 330, 35

Avila-Reese, V. 2006, preprint (astro-ph/0605212)

Avila-Reese, V., Carrillo, A., Valenzuela, O., & Klypin, A. 2005, MNRAS, 361, 997

Avila-Reese, V., Colín, P., Gottlöber, S., Firmani, C., & Maulbetsch, C. 2005, ApJ, 634, 51

Benson, A.J., Frenk, C.S., Lacey, C.G., Baugh, C.M. & Cole, S. 2002, 333, 177

Berentzen, I., Shlosman, I., & Jogee, S. 2006, ApJ, 637, 582

Bershady, M. A., Jangren, A., & Conselice, C. J. 2000, AJ, 119, 2645

Block, D. L., & Puerari, I. 1999, A&A, 342, 627

Boissier, S. & Prantzos, N. 2001, MNRAS, 325, 321

Bournaud, F., & Combes, F. 2002, A&A, 392, 83

Bullock, J.S., Kravtsov, A.V. & Weinberg, D.H. 2000, ApJ, 539, 517

Bureau, M., & Athanassoula, E. 2005 ApJ, 626, 159

Burstein, N., & Heiles, K. 1982, AJ, 87, 1165

Buta, R. & Combes, F. 1996, Fundam. Cosm. Phys., 17, 95

Buta, R. 1986 ApJS, 61, 609

Buta, R. 1995 ApJS, 96, 39

Buta, R. 1999 Ap&SS, 269, 79

Colín, P., Valenzuela, O., & Klypin, A. 2006, ApJ, 644, 687

Cole, S., Lacey, C. G., Baugh, C. M., & Frenk, C. S. 2000, MNRAS, 319, 168

Conselice, C. J. 1997, PASP, 109, 1251

Conselice, C. J. 2003, ApJS, 147, 1 (C2003)

Conselice, C. J., Bershady, M. A., & Gallagher, J. S., III 2000, å, 354, L21

Debattista, V. P., & Sellwood, J. A. 2000, ApJ, 543, 704

de Jong, R., & van der Kruit, P.C. 1994, A&AS, 106, 451

de Jong, R. S. 1996, å, 313, 377

de Vaucouleurs, G., de Vaucouleurs, A., Corwin, H.G., et al. 1991, Third Reference Catalogue of Bright Galaxies, New York, Springer-Verlag

de Vaucouleurs, A., & Longo, G. 1988, Catalogue of visual and infrared photometry of galaxies from 0.5 micrometer to 10 micrometer, University of Texas

Dutton, A. A., van den Bosch, F. C., Dekel, A., & Courteau, S. 2006, ApJ, in press (astro-ph/0604553)

Elmegreen, B.G., & Elmegreen, D.M. 1982, MNRAS, 201, 1021

Erwin, Peter. 2005, MNRAS, 364, 283

Eskridge P. B. et al., 2000, AJ, 119, 536

Firmani, C., & Avila-Reese, V. 2000, MNRAS, 315, 457

Frei, Z., Guhathakurta, P., Gunn, J. E., & Tyson, J. A. 1996, AJ, 111, 174.

Gallagher, J.S., Hunter, D.A. 1986, AJ92, 557

Graham, A. W., Trujillo, I., & Caon, N. 2001, AJ, 122, 1707

Gadotti, D.A., & dos Anjos, S. 2001, AJ, accepted (astro-ph/0106303)

Gnedin, O., Weinberg, D. H., Pizagno, J., Prada, F. & Rix, H.-W. 2006, preprint (astro-ph/0607394)

Giovanelli, R., Haynes, M. P., Salzer, J. J., Wegner, G., da Costa, L. N., & Freudling, W. 1995, AJ, 110, 1059

Godwin, J.G., Bucknell, M.J., Dixon, K.L., Green, M.R., Peach, J.V., & Wallis, R.E. 1977, The Observatory, 97, 238

Hernández-Toledo, H.M., Dultzin-Hacyan D., González, J.J., & Sulentic, J. 1999, AJ, 118, 108

Hernández-Toledo, H. M., Avila-Reese, V., Conselice, C. J., & Puerari, I. 2005, AJ, 129, 682

Hernández-Toledo, H. M., Avila-Reese, V., Salazar-Contreras, J. R., & Conselice, C. J. 2006, AJ, 132, 71

Hubble, E. P. 1936, The Realm of the Nebulae (reprinted 1958; New York: Dover)

Jansen, R.A., Franx, M., Fabricant, D., & Caldwell, N. 2000, ApJS, 126, 271

Karachentsev, I. D., Karachentseva, V. E., Huchtmeier, W. K. 2006, å, 451, 817

Karachentseva, V. E. 1973, Astrof. Issledovanija Byu. Spec. Ast. Obs., 8, 3

Kassin, S. A., de Jong, R. S., & Weiner, B. J. 2006, ApJ, 643, 804

Kauffmann, G., Charlot, S., & Balogh, M.L. 2001, mnras, submitted (astro-ph/0103130)

Kauffmann, G., White, S.D.M., & Guiderdoni, B. 1993, MNRAS, 264, 201

Klypin, A.A., Kravtsov, A.V., Valenzuela, O., & Prada, F. 1999, ApJ, 522, 82

Koopmann, R. A., & Kenney, J. D. P. 2006, ApJS, 162, 97

Lacey, C.G., & Silk, J. 1991, ApJ, 381, 14

Larson, R.B., & Tinsley, B.M. 1978, ApJ, 219, 46

Laurikainen, E., Salo, H., & Rautiainen, P. 2002, MNRAS, 331, 880

Mayer, L., Governato, F., Colpi, M., Moore, B., Quinn, T., Wadsley, J., Stadel, J., & Lake, G. 2001, ApJ, 547, L123

Metcalfe, N., Ratcliffe, A., Shanks, T., & Fong, R. 1998, MNRAS, 294, 147

Moore, B., Katz, N., Lake, G., Dressler, A., & Oemler, A., Jr. 1996, Nature, 379, 613

Moore, B., Ghigna, S., Governato, F., Lake, G., Quinn, T., Stadel, J. & Tozzi, P. 1999, ApJ, 524, L19

Morgan, W. W., & Osterbrock, D. E. 1969, AJ, 74, 515

Okamura, S., Kodaira, K, & Watanabe, M. 1984, ApJ, 280, 7

Park, C., Choi, Y.-Y., Vogeley, M. S., Gott, J. R. I., & Blanton, M. R. 2007, ApJ, 658, 898

Pisano, D. J., Wilcots, E. M., & Liu, C. T. 2002, ApJS, 142, 161

Pizagno, J., et al. 2005, ApJ, 633, 844

Prugniel Ph. 1987, CDS Bull., 33, 17

Prugniel, Ph., & Héraudeau, Ph. 1998, A&AS, 128, 299

Richter, O., & Sancisi, R. å, 290 L 9

Rivolo, A. R., & Yahil, A. 1981, ApJ, 251, 477

Rix, H., & Zaritsky, D. ApJ447 82

Roberts, M.S., & Haynes, M.P. 1994, ARA&A, 32, 115

Rojas, R. R., Vogeley, M. S., Hoyle, F., & Brinkmann, J. 2004, ApJ, 617, 50

Rojas, R. R., Vogeley, M. S., Hoyle, F., & Brinkmann, J. 2005, ApJ, 624, 571

Skrutskie, M. F., Cutri, R. M., Stiening, R. et al. 2006, AJ, 131, 1163

Schlegel, D.J., Finkbeiner, D.P. & Davis, M., 1998, ApJ, 500, 525

Shustov, B., Wiebe, D., & Tutukov, A. 1997, å, 317, 397

Sofue, Y. 1993, PASP, 105, 308

Taylor-Mager, V. A., Conselice, C. J., Windhorst, R. A., Jansen, R. A., preprint (arXiv:astro-ph/0612558v2)

Trentham, N., Möller, O., & Ramirez-Ruiz, E. 2001, MNRAS, 322, 658

Tully, R. B. 1987, ApJ, 321, 280

Tully, R. B., & Pierce, M. J. 2000, ApJ, 533, 744

Tully, R.B., Pierce, M.J., Huang, J., Saunders, W., Verheijen, M.A.W. &Witchalls, P.L., 1998, AJ, 115, 2264

Valenzuela, O., & Klypin, A. 2003, MNRAS, 345, 406

Verheijen, M. A. W. 1997, Ph.D. Thesis,

Wang, B. & Heckman, T.M. 1996, ApJ, 457, 645

Whitford, A.E. 1936, ApJ, 83, 424

Wozniak et al. 1995, A&AS, 111, 115

Yang, X., Mo, H. J. & van den Bosch, F. C. 2003, MNRAS, 339, 1057

Zaritsky, D., Kennicutt, R.C., & Huchra, J.P. 1994, ApJ, 420, 87

Zavala, J., Avila-Reese, V., Hernández-Toledo, H., Firmani, C. 2003, A&A, 412, 633

This 2-column preprint was prepared with the AAS LaTeX macros v5.2.

Table 1

Journal of Observations. The number of frames per filter, the integration time (in seconds), and the mean FWHM for each observation (in arcsec) are given.

CIG	B	$< B >_{\rm FWHM}$	V	$< V >_{\rm FWHM}$	R	$< R >_{\rm FWHM}$	I	$< I >_{\rm FWHM}$
CIG 1	1×1200	2.3	1×600	2.4	1×300	2.1	1×300	2.4
CIG 4	1×1200	2.3	1×600	2.2	1×300	2.0	2×150	1.8
CIG 33	1×1200	2.3	1×600	2.2	1×300	2.3	1×300	2.5
CIG 53	2×1200	2.1	2×600	2.3	2×300	2.0	2×300	1.8
CIG 56	1×1200	2.4	1×600	2.5	1×300	2.3	1×300	2.2
CIG 68	1×1200	2.1	2×300	2.0	2×120	2.0	2×60	2.3
CIG 80	1×1200	2.7	2×300	2.5	1×300	2.6	2×120	1.8
CIG 103	2×1200	2.0	1×600	1.7	1×300	1.8	1×150	1.4
CIG 116	1×1200	2.1	1×600	1.9	2×150	1.6	2×150	1.6
CIG 123	1×1200	2.0	1×600	2.3	2×150	1.9	2×150	2.0
CIG 138	2×1200	2.2	2×600	1.9	3×150	1.8	3×150	2.1
CIG 139	2×1200	2.1	1×600	2.0	1×300	1.8	2×150	1.6
CIG 144	2×1200	3.0	1×600	3.0	1×300	2.8	1×300	2.6
CIG 151	2×1200	2.1	2×900	1.7	2×300	1.8	2×300	1.9
CIG 154	2×1200	1.9	1×600	1.5	1×300	1.5	1×300	1.5
CIG 168	1×1200	1.7	1×600	1.5	1×300	1.5	1×300	1.5
CIG 175	1×1200	1.8	1×600	1.6	1×300	1.7	1×300	1.7
CIG 180	2×1200	1.9	2×600	2.0	1×300	1.7	4×150	1.8
CIG 188	2×1200	1.8	1×900	1.8	2×300	1.7	1×300	1.8
CIG 208	1×1200	1.8	1×900	1.7	1×480	1.7	1×480	1.8
CIG 213	1×1200	1.8	1×600	1.7	1×300	1.7	1×300	1.8
CIG 224	1×1200	1.7	2×600	1.7	1×300	1.8	1×240	1.8
CIG 237	1×1200	1.8	1×900	1.7	1×300	1.7	1×300	1.8
CIG 309	2×600	1.8	2×300	1.7	2×60	1.7	2×60	1.7
CIG 314	1×1200	1.8	1×600	1.7	1×300	1.8	1×300	1.8
CIG 434	1×1200	1.8	1×900	1.7	2×300	1.7	1×600	1.7
CIG 472	1×600	1.8	1×600	1.7	1×300	1.7	1×300	1.7
CIG 518	1×600	1.8	1×600	1.8	1×300	1.8	1×300	1.7
CIG 528	1×1200	1.9	1×600	1.8	1×300	1.8	1×300	1.9
CIG 549	1×600	1.9	1×300	1.8	2×120	1.7	1×120	1.9
CIG 604	1×900	1.8	1×600	1.8	2×120	1.8	1×120	1.7
CIG 605	1×900	1.9	1×480	2.0	2×180	2.0	1×180	1.9
CIG 691	1×900	1.9	1×600	2.0	1×300	2.0	1×300	1.9
CIG 710	1×600	1.9	1×600	2.0	1×300	2.0	1×300	1.9
CIG 889	1×1200	2.0	1×600	2.1	1×300	2.0	2×150	1.9
CIG 906	2×1200	2.3	1×600	2.7	2×300	2.0	2×300	1.8
CIG 910	2×1200	2.3	1×600	2.0	1×300	1.9	1×300	1.8
CIG 911	2×1200	1.6	2×600	1.6	1×300	1.5	1×300	1.6
CIG 935	2×1200	1.6	2×600	1.6	2×300	1.5	2×300	1.6
CIG 976	2×1200	1.7	2×600	1.8	2×300	1.8	2×300	1.9
CIG 983	2×1200	1.6	1×600	1.6	1×300	1.5	2×300	1.6

Table 1—*Continued*

CIG	B	$< B >_{\rm FWHM}$	V	$< V >_{\rm FWHM}$	R	$< R >_{\rm FWHM}$	I	$< I >_{\rm FWHM}$
CIG 1004	2×1200	1.6	1×600	1.6	1×300	1.5	1×300	1.6
CIG 1009	2×1200	1.8	1×600	1.6	1×300	1.9	2×150	1.9
CIG 1023	1×1200	1.5	1×600	1.6	1×300	1.6	3×120	1.6

Table 2
General Data for the Observed Isolated Spiral Galaxies.

CIG	Identif	B mag (LEDA)	Type (LEDA)	B mag (NED)	V_{Rad} (km s^{-1})
CIG 1	UGC 00005	14.08	Sbc	13.97	7243
CIG 4	NGC 7817	12.74	Sbc	12.56	2391
CIG 33	NGC 0237	13.72	SABc	13.70	4136
CIG 53	NGC 0575	13.76	Sc	13.45	3185
CIG 56	NGC 0622	14.08	Sb	13.71	5113
CIG 68	NGC 0718	12.59	Sa	12.59	1683
CIG 80	NGC 0772	10.29	Sb	11.09	2473
CIG 103	NGC 0918	13.07	Sc	13.05	1536
CIG 116	NGC 1050	13.55	SBa	13.47	3989
CIG 123	IC 0302	13.60	Sbc	13.59	5854
CIG 138	UGC 02936	14.76	Sc	15.00	3743
CIG 139	NGC 1507	12.79	SBd	12.89	769
CIG 144	UGC 02988	15.52	Sb	14.90	3868
CIG 151	UGC 03059	15.11	Sd	14.70	4743
CIG 154	UGC 03171	14.84	Sc	14.78	4475
CIG 168	IC 2166	13.24	SABc	13.20	2892
CIG 175	UGC 03580	13.09	SABa	12.71	1439
CIG 180	NGC 2344	12.89	SABb	12.81	1126
CIG 188	UGC 03826	14.59	SABc	14.10	1947
CIG 208	UGC 04054	14.80	Sb	14.30	2175
CIG 213	PGC 022141	14.79	Sa	14.88	6089
CIG 224	NGC 2500	12.22	Scd	12.20	693
CIG 237	UGC 04277	14.82	Sc	14.90	5650
CIG 309	NGC 2775	11.14	Sab	11.03	1347
CIG 314	NGC 2776	12.18	SABc	12.14	2798
CIG 434	UGC 05829	13.73	I	13.73	780
CIG 472	NGC 3596	11.79	SABc	11.95	1267
CIG 518	NGC 4062	11.88	SABc	11.90	939
CIG 528	NGC 4357	13.25	Sbc	13.20	4367
CIG 549	NGC 4651	11.38	Sc	11.39	911
CIG 604	NGC 5377	12.16	Sa	12.24	2044
CIG 605	NGC 5375	12.79	SBab	12.40	2572
CIG 691	NGC 5964	13.33	SBcd	12.60	1555
CIG 710	NGC 6015	11.62	Sc	11.69	1111
CIG 889	NGC 6969	15.33	Sa	14.89	4778
CIG 906	UGC 11723	14.74	Sb	14.70	4928

Table 2—*Continued*

CIG	Identif	B mag (LEDA)	Type (LEDA)	B mag (NED)	V_{Rad} (km s^{-1})
CIG 910	IC 5104	14.33	Sab	14.27	5110
CIG 911	NGC 7056	13.67	SBbc	13.75	5501
CIG 935	NGC 7156	13.29	SABc	13.11	4023
CIG 976	NGC 7328	13.93	Sab	13.98	2886
CIG 983	UGC 12173	13.56	SABc	13.49	4960
CIG 1004	NGC 7479	11.71	SBbc	11.60	2443
CIG 1009	NGC 7514	13.55	Sbc	13.54	5005
CIG 1023	UGC 12646	14.22	Sb	13.99	8143

Table 3

Apparent Magnitudes and Color Indices.

CIG	Log (A)	B	V	R	I	$B-V$	$B-R$	$B-I$
CIG1	1.59	13.92	13.32	12.40	12.08	0.60	1.51	1.83
CIG4	1.62	12.86	11.94	11.30	10.27	0.92	1.56	2.59
CIG33	1.53	13.65	13.06	12.53	11.85	0.59	1.12	1.80
CIG53	1.53	13.65	13.02	12.51	11.81	0.63	1.14	1.83
CIG56	1.59	13.96	13.30	12.71	12.00	0.66	1.26	1.96
CIG68	1.58	12.52	11.67	11.10	10.29	0.84	1.42	2.23
CIG80	1.59	11.65	10.80	10.23	9.38	0.85	1.42	2.27
CIG103	1.58	13.28	12.37	11.68	10.75	0.92	1.60	2.53
CIG116	1.55	13.71	12.81	12.25	11.48	0.90	1.46	2.23
CIG123	1.59	13.81	13.00	12.33	11.60	0.81	1.47	2.20
CIG138	1.59	14.60	13.33	12.51	11.28	1.27	2.09	3.31
CIG139	1.60	12.89	12.36	11.90	11.45	0.52	0.98	1.43
CIG144	1.59	15.31	13.95	13.03	11.63	1.36	2.28	3.68
CIG151	1.57	14.96	14.07	13.34	12.37	0.89	1.62	2.59
CIG154	1.52	14.62	14.05	13.48	12.93	0.58	1.15	1.69
CIG168	1.50	12.68	12.01	11.45	10.86	0.66	1.22	1.82
CIG175	1.50	13.01	12.57	12.08	11.50	0.44	0.92	1.51
CIG180	1.53	12.99	12.14	11.57	10.80	0.85	1.41	2.19
CIG188	1.50	13.20	12.70	12.25	11.99	0.50	0.94	1.20
CIG208	1.50	14.58	14.01	13.55	12.86	0.58	1.03	1.72
CIG213	1.55	14.74	13.80	00.00	00.00	0.94	0.00	0.00
CIG224	1.50	12.06	11.62	11.34	10.85	0.44	0.72	1.20
CIG237	1.50	14.39	13.53	12.95	12.27	0.86	1.44	2.11
CIG309	1.50	11.31	10.39	9.72	9.09	0.91	1.58	2.30
CIG314	1.50	12.26	11.69	11.26	10.77	0.56	0.99	1.49
CIG434	1.50	13.31	13.09	12.84	12.85	0.21	0.46	0.45
CIG472	1.50	12.01	11.49	10.99	10.45	0.51	1.01	1.55
CIG518	1.50	11.90	11.21	10.62	10.03	0.69	1.28	1.90
CIG528	1.50	13.36	12.68	12.14	11.84	0.67	1.21	1.51
CIG549	1.50	11.65	10.92	10.42	9.84	0.73	1.22	1.80
CIG604	1.50	12.39	11.46	10.87	10.25	0.92	1.51	2.13
CIG605	1.50	12.78	12.08	11.65	11.65	0.70	1.13	1.14
CIG691	1.50	12.45	11.82	11.48	10.89	0.63	0.97	1.56
CIG710	1.50	11.69	11.14	10.61	10.08	0.56	1.08	1.61
CIG889	1.57	14.47	13.52	12.84	12.07	0.95	1.63	2.40
CIG906	1.43	14.89	14.09	13.44	12.61	0.81	1.46	2.29

Table 3—*Continued*

CIG	Log (A)	B	V	R	I	$B-V$	$B-R$	$B-I$
CIG910	1.43	14.81	13.82	13.25	12.49	0.99	1.57	2.32
CIG911	1.58	13.86	13.09	12.48	11.75	0.77	1.38	2.11
CIG935	1.56	13.41	12.72	12.24	11.53	0.69	1.17	1.88
CIG976	1.53	13.99	13.10	12.55	11.46	0.89	1.44	2.53
CIG983	1.57	13.81	13.03	12.28	11.64	0.78	1.53	2.18
CIG1004	1.57	11.82	11.04	10.47	9.66	0.78	1.35	2.16
CIG1009	1.35	13.98	13.15	12.55	11.80	0.84	1.44	2.18
CIG1023	1.54	14.08	13.26	12.71	11.73	0.82	1.37	2.35

Table 4

Corrected Colors and Absolute Magnitudes.

CIG	$(B-V)_c$	$(B-R)_c$	$(B-I)_c$	M_B	M_V	M_R	M_I
CIG1	0.36	1.28	1.39	-22.11	-22.47	-23.39	-23.50
CIG4	0.65	1.27	2.08	-21.11	-21.75	-22.37	-23.18
CIG33	0.47	1.00	1.59	-20.68	-21.15	-21.67	-22.26
CIG53	0.54	1.01	1.64	-20.03	-20.57	-21.04	-21.67
CIG56	0.54	1.12	1.73	-20.84	-21.39	-21.96	-22.58
CIG68	0.79	1.34	2.10	-19.65	-20.44	-20.99	-21.75
CIG80	0.64	1.15	1.84	-22.00	-22.64	-23.16	-23.85
CIG103	0.46	0.93	1.53	-20.33	-20.79	-21.26	-21.86
CIG116	0.78	1.31	1.98	-20.60	-21.38	-21.90	-22.57
CIG123	0.54	1.10	1.62	-21.95	-22.49	-23.04	-23.57
CIG138	0.54	1.06	1.75	-22.23	-22.77	-23.29	-23.98
CIG139	0.19	0.57	0.75	-18.59	-18.78	-19.16	-19.33
CIG144	0.53	1.11	1.89	-22.05	-22.58	-23.16	-23.95
CIG151	0.38	0.93	1.53	-21.34	-21.72	-22.28	-22.87
CIG154	0.43	0.93	1.37	-20.01	-20.44	-20.94	-21.38
CIG168	0.44	0.93	1.35	-21.33	-21.77	-22.26	-22.68
CIG175	0.30	0.75	1.23	-19.11	-19.41	-19.86	-20.34
CIG180	0.74	1.25	1.94	-18.52	-19.26	-19.77	-20.46
CIG188	0.40	0.80	0.97	-19.45	-19.84	-20.25	-20.42
CIG208	0.34	0.77	1.28	-18.83	-19.17	-19.60	-20.10
CIG213	0.86	0.00	0.00	-20.30	-21.17	00.00	00.00
CIG224	0.40	0.65	1.10	-18.12	-18.52	-18.77	-19.22
CIG237	0.46	1.02	1.32	-21.99	-22.45	-23.01	-23.31
CIG309	0.83	1.48	2.12	-20.49	-21.32	-21.97	-22.61
CIG314	0.42	0.83	1.21	-21.33	-21.75	-22.16	-22.54
CIG434	0.18	0.42	0.39	-17.05	-17.23	-17.47	-17.44
CIG472	0.48	0.97	1.48	-19.43	-19.91	-20.39	-20.90
CIG518	0.56	1.16	1.65	-19.32	-19.88	-20.48	-20.97
CIG528	0.44	0.96	1.05	-21.59	-22.03	-22.55	-22.63
CIG549	0.65	1.14	1.64	-19.28	-19.93	-20.42	-20.92
CIG604	0.79	1.38	1.86	-20.59	-21.39	-21.98	-22.45
CIG605	0.64	1.05	0.98	-20.34	-20.98	-21.39	-21.32
CIG691	0.53	0.83	1.34	-19.71	-20.24	-20.54	-21.05
CIG710	0.41	0.94	1.33	-19.91	-20.32	-20.85	-21.24
CIG889	0.66	1.30	1.81	-21.05	-21.71	-22.35	-22.86
CIG906	0.50	1.16	1.72	-20.73	-21.22	-21.88	-22.45

Table 4—*Continued*

CIG	$(B-V)_c$	$(B-R)_c$	$(B-I)_c$	M_B	M_V	M_R	M_I
CIG910	0.68	1.17	1.65	-20.97	-21.64	-22.14	-22.62
CIG911	0.66	1.21	1.86	-21.08	-21.74	-22.29	-22.94
CIG935	0.59	1.03	1.67	-20.81	-21.40	-21.84	-22.47
CIG976	0.67	1.17	2.09	-20.12	-20.79	-21.30	-22.22
CIG983	0.50	1.17	1.59	-21.63	-22.12	-22.80	-23.21
CIG1004	0.58	1.08	1.74	-21.72	-22.30	-22.80	-23.46
CIG1009	0.67	1.22	1.84	-20.98	-21.65	-22.20	-22.82
CIG1023	0.68	1.20	2.08	-21.85	-22.53	-23.04	-23.92

Table 5
Final Morphological Classification.

CIG	Type (NED)	Type (This work)	Bars/Rings	Optical Arms	Bar Ellipticity $\epsilon_{\max}$
CIG1	SABbc	SBbc	B	multi	0.24
CIG4	SAbc	SABc	B	multi	—
CIG33	SAB(rs)cd	SB(rs)c	B/R		0.27
CIG53	SB(rs)c	SB(r)bc	B/R	multi	0.59
CIG56	SB(rs)b	SB(r)b	B/R		0.38
CIG68	SAB(s)a	SB(r)a	B/R		0.39
CIG80	SA(s)b	SB(r)b	B/R	multi	0.20
CIG103	SAB(rs)c	SB(r)c	B/R	multi	0.19
CIG116	(R)SB(s)a	RSB(s)a	B		0.42
CIG123	SB(rs)bc	SB(r)c	B/R	multi	0.46
CIG138	SB(s)d	SBc	B	multi	0
CIG139	SB(s)m pec	SB(s)m	B		
CIG144	Sb	SABb	B(peanut?)		—
CIG151	SAdm	SABc	B	multi	—
CIG154	SBcd	SB(r)cd	B/R	multi	0.36
CIG168	SAB(s)bc	SAB(s)cd		multi	—
CIG175	SA(s)a pec	Sa pec			
CIG180	SA(rs)c	SA(r)b	R	multi	
CIG188	SAB(s)d	SB(s)d	B	multi	
CIG208	Sb	SABcd	B		—
CIG213	S0	RSB0	B/R		0.39
CIG224	SB(rs)d	RSBd	B/R	multi	0.40
CIG237	Sc	Sc			
CIG309	SA(r)ab	RS(r)a	R		
CIG314	SAB(rs)c	SAB(rs)c	B/R	multi	—
CIG434	Im	Im	B		0.80
CIG472	SAB(rs)c	SA(rs)c	R	multi	
CIG518	SA(s)c	SB(s)bc	B	multi	0.20
CIG528	SAbc	SA(rs)cd	R	multi	
CIG549	SA(rs)c	SB(rs)c	B/R	multi	0.31
CIG604	(R)SB(s)a	RSB(s)a pec	B(boxy)/R		0.22
CIG605	SB(r)ab	SB(r)b	B/R	multi	0.44
CIG691	SB(rs)d	SB(rs)cd	B/R	multi	0.53
CIG710	SA(s)cd	SB(s)cd	B	multi	0.20
CIG889	Sa	SBa	B(peanut)		—
CIG906	Sb	Sb			

Table 5—*Continued*

CIG	Type (NED)	Type (This work)	Bars/Rings	Optical Arms	Bar Ellipticity $\epsilon_{\rm max}$
CIG910	SBab	SBab	B		—
CIG911	SBb	SB(r)b	B/R	multi	0.47
CIG935	SAB(rs)cd	SAB(rs)c	B/R	multi	—
CIG976	Sab	SA(s)ab		multi	
CIG983	SAB(rs)c	SB(rs)cd	B/R	multi	0.30
CIG1004	SB(s)c	SB(s)c	B	multi	0.60
CIG1009	Sa	S(r)ab	R	multi	
CIG1023	SB(r)b	RSB(r)b	B/R		0.40

Table 6

R Band CAS Parameters for Isolated Spiral Galaxies.

CIG	Inclination	$C(R)$	$A(R)$	$S(R)$
CIG1	66.8	2.88±0.09	0.19±0.02	0.30±0.07
CIG4	84.1	3.30±0.05	0.15±0.02	0.40±0.08
CIG33	54.1	3.13±0.12	0.09±0.21	0.16±0.03
CIG53	34.6	2.57±0.05	0.08±0.02	0.31±0.01
CIG56	51.4	4.19±0.15	0.06±0.01	0.18±0.03
CIG68	32.1	4.85±0.11	0.06±0.01	0.11±0.02
CIG80	48.5	3.66±0.04	0.13±0.01	0.01±0.01
CIG103	57.5	2.84±0.03	0.12±0.03	0.48±0.01
CIG116	47.0	3.62±0.12	0.14±0.07	0.20±0.04
CIG123	49.7	3.18±0.07	0.17±0.02	0.60±0.02
CIG138	78.7	3.65±0.04	0.05±0.03	0.12±0.09
CIG139	90.0	3.30±0.04	0.23±0.02	0.40±0.01
CIG144	90.0	4.32±0.12	0.10±0.03	0.27±0.03
CIG151	90.0	3.17±0.08	0.23±0.04	0.56±0.02
CIG154	37.0	2.90±0.10	0.07±0.03	0.07±0.03
CIG168	57.1	2.71±0.06	0.49±0.01	0.70±0.09
CIG175	63.0	3.94±0.17	0.11±0.02	0.16±0.04
CIG180	26.0	3.69±0.07	0.01±0.02	0.05±0.05
CIG188	36.5	2.62±0.04	0.41±0.02	0.65±0.02
CIG208	90.0	3.83±0.16	0.08±0.03	0.33±0.01
CIG224	21.7	2.89±0.04	0.18±0.03	0.36±0.01
CIG237	90.0	3.90±0.13	0.19±0.08	0.45±0.02
CIG309	40.6	4.13±0.08	0.01±0.08	0.14±0.05
CIG314	58.3	3.42±0.09	0.18±0.02	0.53±0.08
CIG434	24.5	2.81±0.03	0.42±0.07	0.65±0.04
CIG472	23.2	2.96±0.08	0.15±0.01	0.51±0.07
CIG518	68.2	2.97±0.06	0.14±0.02	0.53±0.07
CIG528	73.6	3.49±0.13	0.15±0.02	0.35±0.01
CIG549	53.0	3.58±0.09	0.11±0.03	0.06±0.03
CIG604	70.6	4.73±0.12	0.01±0.01	0.23±0.05
CIG605	42.8	4.62±0.12	0.07±0.03	0.53±0.01
CIG691	40.7	2.51±0.04	0.43±0.02	0.65±0.01
CIG710	67.4	3.22±0.05	0.24±0.01	0.50±0.08
CIG889	90.0	4.09±0.21	0.01±0.06	0.05±0.02
CIG906	90.0	4.09±0.07	0.19±0.03	0.40±0.02
CIG910	90.0	3.75±0.12	0.08±0.02	0.30±0.08

Table 6—*Continued*

CIG	Inclination	$C(R)$	$A(R)$	$S(R)$
CIG911	20.9	3.27±0.12	0.08±0.08	0.11±0.03
CIG935	40.0	3.03±0.08	0.12±0.03	0.19±0.05
CIG976	78.3	3.26±0.10	0.15±0.02	0.41±0.08
CIG983	62.0	2.73±0.06	0.15±0.02	0.17±0.05
CIG1004	36.4	3.31±0.03	0.23±0.08	0.45±0.07
CIG1009	48.7	3.16±0.10	0.05±0.04	0.14±0.04
CIG1023	49.7	4.39±0.17	0.05±0.01	0.20±0.04

Table 7
Magnitudes at Different Circular Apertures.

CIG	$Log A1$	B	V	R	I	$Log A2$	B	V	R	I
CIG1	1.11	14.10	13.41	12.81	12.22	1.41	14.01	13.39	12.65	12.20
CIG4	1.14	13.24	12.31	11.65	10.75	1.44	12.89	11.97	11.33	10.35
CIG33	1.05	13.82	13.19	12.67	12.03	1.35	13.67	13.06	12.54	11.87
CIG53	1.10	14.03	13.34	12.83	12.16	1.35	13.68	13.02	12.52	11.83
CIG56	1.11	14.07	13.37	12.80	12.11	1.41	13.98	13.31	12.73	12.03
CIG68	1.10	12.87	12.03	11.48	10.75	1.40	12.55	11.72	11.16	10.38
CIG80	1.12	12.48	11.57	10.96	10.13	1.42	11.87	11.01	10.41	9.57
CIG103	1.10	14.07	13.12	12.44	11.55	1.40	13.40	12.48	11.80	10.91
CIG116	1.08	13.91	13.04	12.48	11.64	1.38	13.72	12.83	12.27	11.48
CIG123	1.11	14.22	13.31	12.67	11.85	1.41	13.84	13.01	12.37	11.61
CIG138	1.11	15.02	13.80	12.90	11.77	1.41	14.62	13.40	12.53	11.35
CIG139	1.13	13.34	12.80	12.35	11.76	1.43	12.93	12.38	11.93	11.45
CIG144	1.12	15.53	14.18	13.26	12.08	1.42	15.31	13.996	13.06	11.79
CIG151	1.10	15.24	14.32	13.65	12.85	1.40	15.00	14.16	13.49	12.81
CIG154	1.05	14.71	14.09	13.59	12.99	1.35	14.63	14.05	13.52	12.97
CIG168	1.20	13.272	12.571	11.960	11.131	1.50	12.623	11.980	11.386	10.536
CIG175	1.20	13.418	12.861	12.361	11.668	1.50	13.116	12.657	12.195	11.346
CIG180	1.06	13.50	12.61	12.03	11.27	1.36	13.11	12.24	11.67	10.91
CIG188	1.20	13.803	13.309	12.898	12.176	1.50	13.137	12.68	12.255	11.475
CIG208	1.20	14.62	14.007	13.593	12.935	1.50	14.275	13.851	13.478	12.772
CIG224	1.20	12.73	12.212	11.775	11.085	1.50	12.025	11.501	11.127	10.098
CIG237	1.20	14.825	13.849	13.17	12.279	1.50	14.341	13.522	12.936	11.928
CIG309	1.20	11.765	10.831	10.164	9.35	1.50	11.377	10.445	9.778	8.927
CIG314	1.20	12.586	12.0	11.527	10.909	1.50	12.244	11.711	11.245	10.626
CIG434	1.20	14.036	13.787	13.417	13.024	1.50	13.292	13.145	12.809	12.394
CIG472	1.20	12.4	11.822	11.282	10.617	1.50	12.098	11.567	11.042	10.365
CIG518	1.20	12.418	11.677	11.07	10.332	1.50	11.962	11.257	10.665	9.918
CIG528	1.20	13.571	12.79	12.233	11.548	1.50	13.336	12.645	12.135	11.463
CIG549	1.20	12.002	11.235	10.676	9.978	1.50	11.621	10.91	10.381	9.686
CIG604	1.20	12.731	11.844	11.196	10.426	1.50	12.386	11.551	10.917	10.14
CIG605	1.20	13.207	12.337	11.94	11.169	1.50	12.778	11.833	11.555	10.446
CIG691	1.20	13.273	12.609	12.095	11.474	1.50	12.404	11.819	11.363	10.766
CIG710	1.20	12.212	11.62	11.078	10.399	1.50	11.733	11.208	10.682	10.044
CIG889	1.10	14.52	13.53	12.90	12.11	1.40	14.50	13.53	12.88	12.08
CIG906	0.96	15.26	14.33	13.66	12.80	1.26	14.95	14.09	13.44	12.61
CIG910	0.96	14.99	14.08	13.44	12.65	1.26	14.82	13.89	13.28	12.52

Table 7—*Continued*

CIG	$LogA1$	B	V	R	I	$LogA2$	B	V	R	I
CIG911	1.10	13.88	13.16	12.53	11.83	1.40	13.86	13.12	12.49	11.76
CIG935	1.08	13.561	12.866	12.375	11.716	1.39	13.424	12.731	12.245	11.558
CIG976	1.06	14.102	13.29	12.747	11.992	1.36	13.962	13.157	12.623	11.852
CIG983	1.10	14.061	13.265	12.626	11.921	1.40	13.825	13.051	12.336	11.681
CIG1004	1.10	12.916	12.019	11.402	10.583	1.40	12.087	11.27	10.687	9.88
CIG1009	0.88	14.276	13.421	12.853	12.135	1.18	13.989	13.15	12.572	11.831
CIG1023	1.09	14.388	13.511	12.94	12.15	1.39	14.124	13.279	12.724	11.833